Colloids and Surfaces B: Biointerfaces 255 (2025) 114916

Contents lists available at ScienceDirect

Colloids and Surfaces B: Biointerfaces

journal homepage: www.elsevier.com/locate/colsurfb

Biofunctional silk sericin hydrogels: A versatile platform with potential for tissue healing and regeneration

Anabela Veiga [a,b,c,d], Viviana Ribeiro [a], Rosa Ana Ramírez-Jiménez [d,e], Maria Rosa Aguilar [d,e], Luis Rojo [d,e,*], Ana L. Oliveira [a,**]

[a] Universidade Católica Portuguesa, CBQF - Centro de Biotecnologia e Química Fina – Laboratório Associado, Escola Superior de Biotecnologia, Porto, Portugal
[b] LEPABE-Laboratory for Process Engineering, Environment, Biotechnology & Energy, Department of Chemical Engineering, Faculty of Engineering of the University of Porto, R. Dr. Roberto Frias, Porto 4200-465, Portugal
[c] ALiCE-Associate Laboratory in Chemical Engineering, Faculty of Engineering, University of Porto, Rua Dr. Roberto Frias, Porto 4200-465, Portugal
[d] Instituto de Ciencia y Tecnología de Polímeros (ICTP) CSIC, C. Juan de la Cierva, 3, Madrid 28006, Spain
[e] Centro de Investigación Biomédica en Red de Bioingienería, Biomateriales y Biotecnología CIBER-BBN, Instituto de Salud Carlos III, Calle Monforte de Lemos S/N, Madrid 28029, Spain

ARTICLE INFO

Keywords:
Horseradish peroxidase (HRP)
Hydrogels
Silk sericin (SS)
Skin tissue engineering (TE)
Tannic acid (TA)

ABSTRACT

Discarded silk sericin protein (SS) presents a high yet underexplored potential as a biomaterial for tissue engineering (TE). Despite its biocompatibility, antioxidant activity, and moisture retention properties, its poor stability in aqueous media has limited broader application. In this work, we developed and characterized SS-based hydrogels using tannic acid (TA) and horseradish peroxidase (HRP) crosslinking systems to address these limitations and expand their use in skin TE. Hydrogels were prepared using SS concentrations of 2.5 % and 5 % (w/v) and evaluated for rheological behavior (G′ ranging from 100 to 10,000 Pa), swelling (up to 24 %), retention capacity (stable over 24–30 h), and degradation in proteolytic environments (mass loss ranging from ~0–11 %, depending on formulation). TA-crosslinked hydrogels showed strong fluid retention and are suitable for high-moisture 3D wound dressings and coating applications. HRP-crosslinked hydrogels demonstrated tunable mechanical properties, shear-thinning behavior, and full recovery post-deformation, making them ideal for use as bioinks in 3D bioprinting and injectable matrices. *In vitro* assays confirmed cytocompatibility, with viability exceeding 85 %, and successful cell encapsulation and proliferation. Overall, this study presents a versatile SS-based hydrogel platform with potential for various biomedical applications, particularly in skin tissue healing and regeneration.

1. Introduction

In response to the challenges posed by an aging population and the need for cost-efficient approaches, developing new materials for skin tissue engineering (TE) is crucial. Apart from the potential benefits for society, the sector represents a growing market worldwide. Conventional synthetic solutions exhibit drawbacks, including high costs and limited biocompatibility. To address these issues, researchers have been focusing on natural-based materials, aligning with the goals of sustainability in biomedical applications [1–3]. In this context, hydrogels derived from natural materials are receiving increasing attention in the field of skin-TE due to their intrinsic properties such as biocompatibility, biodegradability, tunability, and functionalization, including silk sericin (SS) [4,5].

SS is a highly hydrophilic protein that contains 18 amino acids, including serine (≈32 %), aspartic acid (≈18 %) and glycine (≈16 %) [6]. This natural protein can promote cell adhesion and proliferation of mammalian cells [7,8], stimulate collagen production [9] and act as a nutritive media for cell growth [10]. SS also provides moisturizing and antioxidant properties, which are important for skin-related applications [11]. Moreover, it can be obtained through a simple extraction process using boiling water, without the need for hazardous solvents or reagents, making it environmentally friendly and suitable for biomedical applications [12].

* Corresponding author at: Instituto de Ciencia y Tecnología de Polímeros (ICTP) CSIC, C. Juan de la Cierva, 3, Madrid 28006, Spain.
** Corresponding author.
E-mail addresses: rojodelolmo@ictp.csic.es (L. Rojo), aloliveira@ucp.pt (A.L. Oliveira).

https://doi.org/10.1016/j.colsurfb.2025.114916
Received 5 January 2025; Received in revised form 20 June 2025; Accepted 26 June 2025
Available online 4 July 2025

This protein was long considered merely a by-product of silk processing, and most of the scientific evidence has only emerged over the past two decades [13]. However, several aspects remain to be explored, particularly when compared with silk fibroin (SF) materials, which are already well-established in the literature [14]. One of the main concerns regarding the use of SS is its batch-to-batch variability and the effects of different concentrations and post-degumming sterilization methodologies. In a recent study, our research team compared various concentration techniques and proposed a new method involving cryo-lyophilization followed by supercritical sterilization (sCO_2), which preserves the intrinsic properties of SS [15]. This approach opens new avenues for the development of novel 3D materials by leveraging its inherent gelation properties [16,17].

Low SS concentrations (2.5 – 4 wt% (w/v)) have been demonstrated as optimal for 3D printing [18–20], while higher concentrations (5 – 14 wt%) showed applicability for *in vivo* or *in situ* applications [21,22]. However, its low mechanical strength and poor stability in aqueous medium (due to solubility) restrict its widespread applicability in the biomedical field [23,24]. Moreover, although SS has shown promising biological properties, its relatively recent introduction in the biomedical field presents challenges in meeting stringent regulatory standards. These limitations may delay its clinical translation [25]. A common strategy to address such issues involves the use of crosslinking methods to improve the structural stability and performance of SS-based materials. [26,27].

Several strategies have been employed for the development of crosslinked SS hydrogels, such as the addition of ethanol [28] and water-soluble polymers such as polyvinyl alcohol (PVA) [29]; the addition of crosslinking agents such as glutaraldehyde [30]; and methacryloyl modification for *in situ* stabilization, facilitated by UV light irradiation [31]. Most of these systems involve blending with other polymers (which can induce changes in SS conformation), the use of harsh complex chemistries, or exhibiting slow gelling kinetics that may not be compatible with cell incorporation [32,33]. Considering these challenges, the exploration of simpler approaches holds potential where mild reaction conditions avoid harm to sensitive biological components [34,35]. Rapid gelation is particularly beneficial for skin-TE applications. Furthermore, eco-friendly crosslinking agents sourced from renewable materials resonate with a focus on environmentally responsible practices and green chemistry principles [36,37].

Tannic acid (TA), a natural plant-derived polyphenol, is being used as a crosslinking agent to develop new hydrogel systems [38]. TA contains both pyrogallol and catechol groups on a central glucose core enabling surface functionalization, or material interactions through molecular complexing, crosslinking, and a variety of non-covalent interactions [39]. In recent studies, TA has also enabled the design of highly stretchable and self-healing hydrogels through interpenetrating networks and reversible bonding mechanisms, with implications in wearable and biomedical devices [40].

In addition, TA is biocompatible and has antioxidative, antibacterial, and anti-inflammation properties, making it an excellent natural source for biomaterial development and modification [41]. Although TA addition in SS hydrogels has not been reported, the incorporation of phenolic groups is of interest for wound healing [42,43]. Similar TA-based systems have been reported to provide antibacterial and adhesive properties as well as controlled drug release under wound-like conditions, reinforcing their relevance for biomedical coatings [44].

In a previous work, a SS/TA mixture was used as a 2D coating on titanium surfaces, revealing negligible toxicity to L929 cells and good anti-bacterial properties [45]. TA effect on 3D matrixes has been reported in SF/TA hydrogels with enhanced antimicrobial and antioxidant activities, leading to a significant improvement in wound healing in a full-thickness skin defect model on mice [41]. These hydrogels are based on non-covalent interactions, which results in lower mechanical strength, making it challenging to engineer hydrogels with defined geometrics and limitations in mechanically demanding applications [46]. Moreover, the amount of TA decreased the gelation time in SF-based hydrogels and resulted in a more compact and adherent network structure with a smaller pore size [47]. SF/TA hydrogels were reported to exhibit antioxidant and antibacterial activity, attributed to the sustained release of TA, in particular for the highest concentration (0.7 % wt.), which promoted wound healing when used in a full-thickness skin wound mouse model. The effect of TA concentration (0–3 % wt.) on the development of a collagen hydrogel has also been reported [48]. A TA concentration of **0.5 %**wt. increased the stability of the hydrogels, which maintained their shape and mechanical strength. Biological tests with embedded cells revealed that while 1 % wt. TA provided a suitable microenvironment for cells to maintain viability, lower concentrations (0.1 – **0.5 %** wt.) were adequate to induce proliferation of preosteoblasts (MC3T3-E1) (Supplementary information - 1) (SI-1).

While TA confers beneficial properties for tissue engineering and stabilizes the network through non-covalent interactions, its inherent non-covalent nature may limit the hydrogel's long-term stability. In this context, horseradish peroxidase (HRP)/hydrogen peroxide (H_2O_2)-mediated crosslinking has been shown to enhance structural integrity without compromising the biological performance of the resulting materials. HRP/H_2O_2 crosslinking is proposed to form covalent bonds between the tyrosine groups on SS to improve hydrogel mechanical stability and the resulting biological properties [49]. According to previous works, the addition of HRP/H_2O_2 crosslinking system to SS results in fast-gelling hydrogels with antioxidant properties. In addition, the hydrogels also promoted cell adhesion and proliferation of L929 fibroblasts [32]. *In vivo* tests have also been conducted in a diabetic mice model, resulting in reduced granulation tissue, decreased wound edge distance, and wound thickness when compared to Tegaderm, a dressing that is commonly used in the clinic [32,33].

Thus, these two crosslinking strategies were selected due to their complementary properties: TA offers antioxidant and bioactive enhancement via non-covalent interactions, while HRP enables rapid covalent crosslinking and structural reinforcement. The objective of the present research was to develop, study, and compare the physicochemical properties and cytocompatibility of SS-crosslinked systems employing both TA and HRP/H_2O_2. For the first time, our work utilized the previously reported cryo-lyophilization followed by sCO_2 sterilization methodology, which enabled us to obtain an off-the-shelf sterile SS raw material that can be easily dissolved and implemented in the development of these 3D structures [15]. The effects of varying SS concentrations (2.5 and 5% wt.), TA concentrations (TA1: 0.05%–0.05% wt., TA2: 0.1%–0.1% wt., TA3: 0.2%–0.2% wt.), and validated HRP (0.2%–0.2% wt.)/H_2O_2 (1%–1% v/v) conditions, as previously described [32], were analyzed. HRP/TA2 hybrid crosslinking was also tested. The hydrogels obtained yielded distinct properties, and their potential for skin tissue engineering was explored.

2. Materials and methods

2.1. Development of sericin-based hydrogels

Preparation of silk sericin (SS) solution: SS from *Bombyx mori* silkworm was extracted by a procedure previously developed and optimized [21]. Briefly, clean-cut cocoon fragments, acquired from a sericulture at APPACDM (Portuguese Association of Parents and Friends of the Mentally Handicapped Citizen of Castelo Branco, Castelo Branco, Portugal), were immersed in deionized water in a proportion of 1:100 (w/v) at boiling temperature for 60 min. The extracted silk-SS solution was then freeze-dried following the methodology reported in a previous work [15]. Before use, the SS powder was dissolved in phosphate buffer solution (PBS) to obtain SS solutions of 2.5 and 5 % wt.: termed SS1 and SS2 respectively. Preliminary tests indicated that this concentration range is optimal for achieving a balance between mechanical integrity and structural stability: higher concentrations yielded an excessively

rigid matrix, while lower concentrations resulted in hydrogels that rapidly degraded and disintegrated [50].

To investigate the potential of tannic acid (TA) as a binder to induce the gelation of SS solutions, a series of SS (**2.5 %** wt.)/TA solutions with varying concentrations of TA (0.05 – **0.7 %** wt.) were prepared at pH 7. Preliminary tests revealed that TA concentrations above **0.5 %**wt. resulted in SS hydrogels with a white, rigid, and inhomogeneous complex, whereas lower TA concentrations yielded more homogeneous hydrogels, albeit with a gradual decrease in permeability as the TA concentration increased. Based on these results, stable hydrogels (0.05, 0.1 and **0.2 %**wt. TA) were selected to conduct further tests.

SS/HRP was also prepared based on enzymatically crosslinked SS hydrogels, in which HRP (0.2 % wt.) and hydrogen peroxide (H_2O_2) (1 % v/v) prepared in PBS were used as crosslinking agents, adapted from a previously developed protocol [51]. Moreover, a formulation using both crosslinkers was also developed to investigate the effect of double crosslinking on the final properties of the hydrogel (SS/TA-HRP). The formulations evaluated are described in Table 1.

After conducting preliminary tests, three different concentrations (TA1:0.05, TA2:0.1, and TA3:**0.2 %** wt.) were chosen for further characterization, excluding heterogeneous and highly stiff formulations.

2.2. Physicochemical characterization

2.2.1. Rheological characterization and Fourier transform infrared spectroscopy

Rheology experiments were performed at a controlled temperature of 37ºC, using a rheometer (ARG2, TA Instruments, New Castle, DE, USA) equipped with a cone-plate cross-geometry (20-mm diameter) fitted at a 1000 μm gap. Sample preparation included pouring approximately 1 mL of a formulation into a spherical Teflon mold with a diameter = 2 cm and storing it in the fridge for 24 h at 4 ºC. The viscoelastic properties of the stabilized SS-based formulations were evaluated through frequency sweeps (0.1 – 1000 Hz) at a low strain amplitude (1 %), within the linear viscoelastic range (**SI-2**) [21]. Flow sweep tests were also conducted for viscosity rotational shear measurements at an increasing shear rate from 0.1 to 10000 s^{-1}. At least two replicates of each sample were recorded for each test and the data presented is the average of these measurements.

The response to oscillatory shear stress was also evaluated by subjecting the 3D hydrogels to repeated cycles of shear stress. A low shear strain (1 %) at 1 Hz was applied for 5 min (as defined in previous time sweep experiments). Then, an increase of the shear strain to 1000 % was applied for 200 s to rupture the gel. Finally, reduction to the same rate as the initial shear strain was implemented for 5 min to allow stabilization (recovery of the gel network).

Attenuated total reflection-Fourier Transform Infrared Spectroscopy analysis (ATR-FTIR) spectroscopy was employed after the hydrogels were dried at room temperature with a PerkinElmer Spectrum Two spectrophotometer. The spectra were obtained using 4 accumulations and a 4 cm^{-1} resolution in the region of 4000 −400 cm^{-1}. Smoothing, ATR baseline correction, and spectra normalization were performed using PerkinElmer Spectrum 10 Spectroscopy Software. FTIR Amide I spectral deconvolution was carried out using Origin 2024b's Peak Deconvolution module. A second derivative approach was employed to reveal hidden peaks by analyzing the terminal derivatives of the spectrum, ensuring that subtle features not immediately visible in the raw data were identified. The Savitzky–Golay smoothing algorithm was applied with a polynomial order of 2, and a window size of 20 points, effectively reducing noise while preserving key spectral details. Finally, peaks were filtered based on their relative height, expressed as a percentage of the most intense peak, so that only significant spectral features were retained, thereby minimizing the contribution of noise and insignificant peaks.

Table 1
Silk SS-based hydrogel formulations containing TA and enzymatically crosslinked with HRP/H_2O_2.

Core material (SS) (% wt.)	TA (% wt.)	HRP/H_2O_2	Sample name
SS1: **2.5 %**	0.05	-	SS1/TA1
	0.1		SS1/TA2
	0.2		SS1/TA3
	-	H_2O_2 (1 % v/v) + HRP (0.2 % wt.)	SS1/HRP
	0.1		SS1/TA2-HRP
SS2: **5 %**	0.05	-	SS2/TA1
	0.1		SS2/TA2
	0.2		SS2/TA3
	-	H_2O_2 (1 % v/v) + HRP (0.2 % wt.)	SS2/HRP
	0.1		SS2/TA2-HRP

2.2.2. Swelling ratio and enzymatic degradation

To perform swelling and degradation studies in simulated physiological conditions, the different hydrogel formulations were prepared by casting 2 mL in spherical Teflon molds with dimensions of 20 mm in diameter and approximately 4.5 mm in height. After gelling in the fridge overnight, a biopsy punch (8 ×20 mm, stainless steel, Williams Medical Supplies, Rhymney, United Kingdom) was used to obtain cylindrical hydrogels (n = 3). These 3D gels were placed in grid mesh containers to weigh at defined time points. The swelling ratio was tested with samples in 50 mL tubes of PBS or ultrapure water placed in an incubator at 37 °C. The wet weight of the samples was measured at 1, 2, 4, and 6 h. At each time point, the swelling ratio was calculated according to the following equation (Eq. (1)):

$$swelling\ ratio(\%) = \frac{w_t - w_d}{w_d} \times 100 \quad (1)$$

where w_t is the wet weight of the sample tested at different time points and w_d corresponds to the initial dry weight of the hydrogel after gelation.

The retention capacity, which is the ability of the hydrogel to retain PBS within its structure over time post-removal from the swelling medium, was evaluated after 24 h of immersion at 37 °C. The samples were weighed after the immersion process (w_w). The wet weight of the samples (w_t) was measured at this point and after being placed in plates at 37 °C, every hour until 30 h. The water retention ratio was calculated according to Eq. (2):

$$retention\ capacity(\%) = \frac{w_t - w_w}{w_w} \times 100 \quad (2)$$

To perform degradation assays, the hydrogels were tested in PBS and PBS with protease Type XIV from *Streptomyces griseus* (3.5 units/mg solid powder, Sigma Aldrich, St. Louis, MO, USA) at 3.2 U/mg and a temperature of 37 °C, according to previous work [21,52]. The wet weight of the samples was measured at 1, 3, 24, 50 h. The degradation ratio at each time point was calculated using the following Eq. (3):

$$degradation(\%) = \frac{w_i - w_t}{w_t} \times 100 \quad (3)$$

where w_i is the initial weight of the hydrogel and w_t is the final weight of the dry specimen at the different time points.

2.2.3. Antioxidant properties

The different SS-based hydrogel formulations (1 mL) were placed in 15 mL Falcons tubes with 2 mL of medium and kept at 37ºC with shaking. After 1, 3, and 7 days, the extracts were collected and stored at −20ºC. To study antioxidant potential, the extracts (n = 5) were used and assessed based on published procedures after mixing with ethanol (3:2) [53]. Radical scavenger activity (RSA) was determined by the reduction in the absorbance of 1,1-diphenyl-2-picrylhydrazyl (DPPH, Merch KGaA, Darmstadtm Germany), dissolved in ethanol: water at the

same ratio (3:2) at a concentration of 0.2 mmol/L. Vitamin C (Fluka, Chemika 95210, Buchs, Switzerland), was prepared in the same conditions at a concentration of 50 μg/mL as a reference [54]. The resulting extracts and DPPH reagent were placed into a 96-well plate in a proportion 1:1 under dark conditions and left to react at room temperature for 30 min and 1 h before measuring the absorbance at 515 nm. RSA was calculated according to Eq. 5:

$$\mathrm{RSA}(\%) = \frac{A_{515}DPPH - A_{515}extract}{A_{515}extract} \times 100 \quad (4)$$

where $A_{515DPPH}$ and $A_{515\ extract}$ are the absorbance at 515 nm of the DPPH and extract solutions respectively.

2.3. In vitro studies

2.3.1. Sample preparation

After lyophilization, the SS powder was sterilized by sCO_2 using the methodology validated in previous work [15]. Briefly, sterilization pouches with SS powder were placed inside a pressure vessel of a 2L-stainless steel autoclave (Eurotechnica GmbH, Bargteheide, Germany). Premium CO_2 Liquid Premier with **99.995 %** purity was used (50 g/min, 140 bar, 39 ºC, 700 rpm).

The sterilized powder was dissolved in PBS inside a laminar flow chamber using a heating plate at 100 °C and a stirring magnet at 400 rpm. After complete dissolution, the SS solution with defined concentration (SS1: 2.5 and SS2: 5 wt%) was added to the previously sterilized crosslinking agents by filtration (0.22 μm sterile membrane filter, Sigma-Aldrich) and vortexed for 5 s (**SI-3**). The hydrogels were stored overnight in the fridge to allow stabilization. Before further use for indirect and direct contact *in vitro* assays, the different experimental conditions were incubated at 37ºC for 30 min.

2.3.2. Indirect contact assay

Cytotoxicity of hydrogels was assessed through an indirect contact test with AlamarBlue® reagent (Invitrogen, USA). A volume of 1 mL of each SS-based hydrogel formulation was placed in a Falcon tube and 2 mL of DMEM was added after gelation and kept at 37 ºC with shaking. After 1 day, the extracts were collected and stored at −20 ºC.

Human dermal fibroblasts (HDFs) (Innoprot, P10856, San Sebastian, Spain) were seeded in 96 well-plates with a cell density of 1×10^5 cells/well using basal medium consisting of Dulbecco's modified Eagle's medium (DMEM) – low glucose enriched with 110 mg/L of sodium bicarbonate and supplemented with 20 % v-v of fetal bovine serum (FBS, Gibco, Grand Island, NY, USA), 200 mM L-glutamine, 100 units/mL penicillin and 100 mg/mL streptomycin. Incubation was carried out at 37 ºC, 95 % humidity, and 5 % CO_2. After 24 h of initial cell seeding, the medium was removed and 100 μL of the previously collected extracts were added to each well and incubated for 24 h. Then, the extracts of the plates were removed and 100 μL of AlamarBlue® reagent at 10 % (v:v) in medium without phenol red was added per well, incubated for 3 h, and fluorescence recorded at an excitation wavelength of 560 nm and an emission wavelength of 590 nm using a Biotek Synergy HT plates (Biotek Instruments, USA). A negative control was prepared by incubating the cells with 20 % DMSO in a culture medium. Data was analyzed as mean ± standard deviation with n = 8 for each bar. Cytotoxicity of the cells was assessed following the ISO 10993–5 standard, which specifies that for a material to be considered cytocompatible, it should demonstrate a cell viability exceeding 70 % when compared to the positive control with 2D cultured HDFs (Eq. (5)).

$$\textit{Cell viability}(\%) = \frac{\textit{Mean Absorbance of hydrogels seeded with cells} - \textit{Mean Absorbance hydrogels}}{\textit{Mean Absorbance of Control Cells} - \textit{Mean Absorbance Control Medium}} \times 100 \quad (5)$$

2.3.3. Direct contact assay

SS1/HRP, SS1/TA2, SS1/TA2-HRP, SS2/HRP, SS2/TA2, SS2/TA2-HRP were selected to conduct direct contact assays. A volume of 300 μL per well was placed in 48 well plates. The HDFs were seeded in each well at 5×10^5 cells/100 μL cell suspension. After incubating for 40 min, 300 μL of DMEM was added to each well. The cells were cultured on the hydrogels for 1, 3, and 7 days with DMEM at 37 °C in 5 % CO_2 with medium replacement every 3 days. Control hydrogels without cells were used as blank.

Cell viability, metabolic activity, and proliferation: metabolic activity in the SS-based hydrogels was determined by the AlamarBlue® assay. After 1, 3, and 7 days of culture, 500 μL of 10 % (v:v) AlamarBlue® solution in medium without phenol red was added to each well. After 6 h of incubation, 100 μL of AlamarBlue® solution was transferred to a 96-well cell culture plate (Greiner Bio-one, Frickenhausen, Germany) in triplicate. Fluorescence was measured as described above (Excitation/emission wavelength of 560/590 nm) using Biotek Synergy HT plates. AlamarBlue data was analyzed as mean ± standard deviation for each bar.

For DNA quantification, (Quant-iT™ PicoGreen™, Thermo Fisher, Waltham, MA, USA) after 1 and 7 days of cell culture, SS1/TA2, SS1/HRP, and SS1/TA2-HRP were washed with sterile PBS and transferred into Eppendorf tubes containing 1 mL of ultrapure water and stored at −80 °C. Samples were placed in liquid nitrogen followed by immersion in a thermostatic bath at 37ºC. After thawing, the hydrogels were subjected to a sonication bath for 1 h to ensure the release of all contents into water [55]. Before DNA quantification, the samples were subjected to vortexing at maximum rpm for 30 s. Afterward, the PicoGreen protocol was followed according to the manufacturer's specifications: in a 96-well plate 10 μL of sample or standard (n = 3), 100 μL of PicoGreen solution, and 90 μL of Tris-EDTA 334 (TE) buffer were added. The plate was covered with aluminum foil and incubated for 10 min at 37ºC. Subsequently, fluorescence was read in a microplate reader using an excitation wavelength of 480 nm and an emission wavelength of 520 nm. The amount of DNA was calculated by interpolation from a standard curve prepared with double-stranded DNA (dsDNA) concentrations from 0 to 2000 ng/mL [56]. Cell-free (thus, DNA-free) gels were used as controls.

Cell viability and proliferation were further assessed through Live/Dead assay (LIVE/DEAD™ Cell Imaging Kit (488/570), Thermo Fisher). According to the protocol, DMEM was removed from the wells and 80 μl of reagent prepared by adding an equal volume of the probe to DMEM, was added. After incubating for 15 min (37 °C and 5 % CO_2), the seeded hydrogels were collected after 1 and 7 days with a spatula, washed with PBS, and placed on a coverslip. A cross-section was made with a scalpel to visualize the cells within the hydrogels. To prevent the hydrogel from dehydration, DMEM was added to the gels using a dropper.

Confocal analyses were performed to evaluate cell morphology at 1 and 7 days of cell culture. The samples were stained with F-actin Phalloidin for the shape and structure of the cell and with DAPI for the nuclei. Briefly, samples were washed with PBS and fixed for 30 min in a 4 % formalin solution at room temperature (RT). After fixation, the samples were washed with water and stored in sterile ultrapure water. Before observation, samples were permeabilized with 0.2 % Triton X-100 (Sigma) for 7 min and then incubated with the conjugated probe phalloidin/Alexa Fluor® 594 (Molecular Probes-Invitrogen, Eugene, OR, USA, 1:40, 1 h at RT) for F-actin staining. Samples were subsequently washed three times with PBS and nuclei were counterstained

with 40,6-diamidino-2-phenylindole dihydrochloride (DAPI, Sigma-Aldrich, Saint Louis, MO, USA, 0.1 mg/mL) in vectashield (Vector laboratories, Newark, CA, USA), just before visualization. The stained samples were observed under laser scanning confocal microscopy–Zeiss LSM900 confocal microscope (Zeiss, Jena, Germany). The scanned z-series were projected onto a single plane using ZEN Microscopy Software (Zeiss, Jena, Germany).

2.3.4. Cell embedding

HDFs were loaded in the different SS1-hydrogel formulations (SS1/TA2, SS1/HRP, SS1/TA2-HRP). These softer hydrogels were expected to be more suitable for embedding cells. An HDF-cell pellet containing 5×10^5 cells was prepared. Each SS-based solution (1 mL) was mixed with the crosslinker and placed in the chamber at 37 °C for 5 min to allow temperature stabilization before cell contact. The cell pellet was mixed with 300 μL of hydrogel solution and transferred into a 48-well plate. After incubating for 40 min (37 °C and 5 % CO_2), to allow gel formation, DMEM was added at 800 μL per well. Cellular metabolic activity was evaluated by AlamarBlue assay on days 1, 3, and 7 (n = 4). The formulation that better preserved cell viability (SS1/HRP) was further evaluated after 14 days. Immunostaining was performed at 7 and 14 days after cell embedding to assess the distribution and proliferation of the HDFs. 3D samples were fixed using histological tissue fixative (Formalin 10 %) (Sigma Aldrich) for 2 h. Following PBS rinsing, the

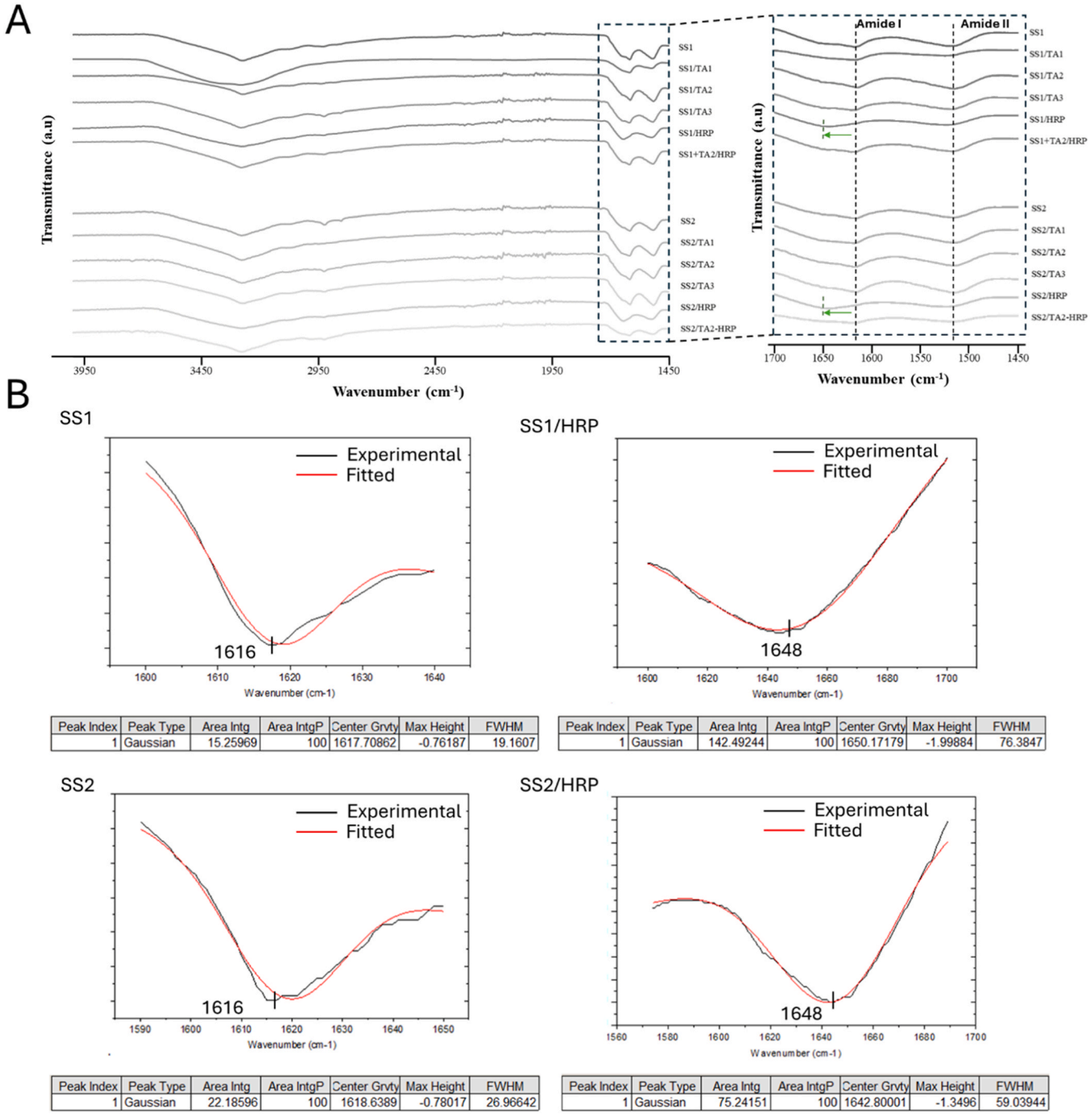

Peak Index	Peak Type	Area Intg	Area IntgP	Center Grvty	Max Height	FWHM
1	Gaussian	15.25969	100	1617.70862	-0.76187	19.1607

Peak Index	Peak Type	Area Intg	Area IntgP	Center Grvty	Max Height	FWHM
1	Gaussian	142.49244	100	1650.17179	-1.99884	76.3847

Peak Index	Peak Type	Area Intg	Area IntgP	Center Grvty	Max Height	FWHM
1	Gaussian	22.18596	100	1618.6389	-0.78017	26.96642

Peak Index	Peak Type	Area Intg	Area IntgP	Center Grvty	Max Height	FWHM
1	Gaussian	75.24151	100	1642.80001	-1.3496	59.03944

Fig. 1. A) ATR-FTIR spectra of the studied SS-based hydrogels (SS/TA, SS/HRP, and SS/HRP-TA) with different SS concentrations (SS1: **2.5 %** wt. and SS2: **5 %** wt.), and identification of the Amide I and Amide II vibrational bands; B) Amide II peak deconvolution for SS1, SS2, SS1/HRP and SS2/HRP formulations.

samples were stored at 2–4°C. Samples were treated with permeabilization buffer (1 % v/v TritonTM X-100 from Sigma-Aldrich in PBS) for 10 min, followed by three washes with PBST (1 % v/v TWEEN® 20 from Sigma-Aldrich in PBS). To minimize non-specific binding, samples were incubated in a blocking buffer (1:10 ratio in PBS, Abcam) for 30 min at RT. Samples were incubated in Alexa Fluor 594 phalloidin (1:400 dilution, Invitrogen) for 45 min, and DAPI (1:1000 dilution, Thermo Scientific) for 10 min, with PBST rinses between steps. Bright-field and fluorescent images were captured using a Keyence All-in-One Fluorescent Microscope (BZ-X710, Keyence Corp, Osaka, Japan).

2.3.5. Statistical analysis

Statistical analysis of indirect and direct contact biological tests was performed with GraphPad Prism 9.0 (GraphPad Software) using One-way ANOVA or 2-way ANOVA test followed by Tukey's method as a Multiple Comparison posthoc test. The significance level was *$p < 0.05$, **$p < 0.01$, ***$p < 0.001$, **** $p < 0.0001$.

3. Results and discussion

3.1. Physicochemical characterization

3.1.1. Chemical structure

FTIR spectra of the studied SS-based hydrogels (SS/TA, SS/HRP, and SS/HRP-TA) with different SS concentrations (SS1: **2.5 %** wt. and SS2: **5 %** wt.), are presented in Fig. 1 to provide qualitative information about the tested samples. The characteristic peaks of amide I (1600 −1690 cm $^{-1}$), are associated with the C═O stretching vibration andamide II (1480–1575 cm $^{-1}$) from N-H bending vibrations, and C-N stretching vibrations [57,58] (Fig. 1A).

The amide I band has been widely used to quantify the secondary structural composition of proteins and polypeptides because of its sensitivity to small variations in molecular geometry and hydrogen bonding patterns [59].

According to the FTIR results obtained (Fig. 1**A**), the Amide I peak appears to be the same for the different formulations tested, with the exception of the HRP-containing formulations (SS1/HRP and SS2/HRP), which exhibit a slight shift to higher wavenumbers. Amide I peak deconvolution confirmed that (Fig. 1**B**), while SS1 and SS2 present the peak at ≈ 1616 cm^{-1} , SS1/HRP and SS2/HRP display the peak at ≈ 1648 cm^{-1} .

Infrared absorptions from α-helices, β-sheets, and random coils typically occur at about 1648–1660, 1625–1640, and 1640–1648 cm^{-1} , respectively [60]. Consequently, these results may suggest that the SS-based hydrogels have a higher β-sheet content, whereas SS1/HRP and SS2/HRP exhibit increased random coil content [61]. However, it is also important to consider that the samples were dried prior to analysis and that this process, together with the influence of the crosslinkers, may account for these observed changes. Therefore, while the data obtained might not exactly reflect the behavior of the hydrogels in their hydrated state, they indicate that the functional groups responsible for the Amide I vibration remain intact following crosslinking.

Adsorbed water between 3800 and 3000 cm^{-1} is identified for all samples and can be overlapped with hydroxyl groups (O-H) H-bonded and C-H bonds, also characteristic of TA and HRP.

3.1.2. Rheological behavior

Mechanical stiffness or elasticity of hydrogels impacts a variety of cellular processes, such as adhesion, proliferation, spreading, migration, and differentiation [62,63]. For all the experimental conditions storage modulus (G') > loss modulus (G''), showing low-frequency dependence (Fig. 2), verifying the formation of crosslinked hydrogels.

The conditions with TA are those with higher G′. Moreover, a direct relationship between increasing TA concentration and increasing G′ was observed, with a G′ of TA3 (0.2 % wt.) > TA1 (0.05 % wt.). The lowest G′ value was attributed to HRP and increased with the addition of TA (SS/TA-HRP formulations).

While TA interacts through hydrogen-bonding mechanisms and hydrophobic effects [64], HRP catalyzes covalent crosslinking reactions, making it suitable as an injectable hydrogel [65]. The polymeric components of tannin can reinforce the phenolic network of SS [66]. The addition of TA to silk can lead to a more compact network structure, due to higher crosslinking [41]. In addition, TA can improve gelation and mechanical properties and *in vitro*/stability. On the other hand, HRP/H_2O_2 G' can be increased by increasing the H_2O_2 concentration. An increase in H_2O_2 would increase available phenolic radicals, which in

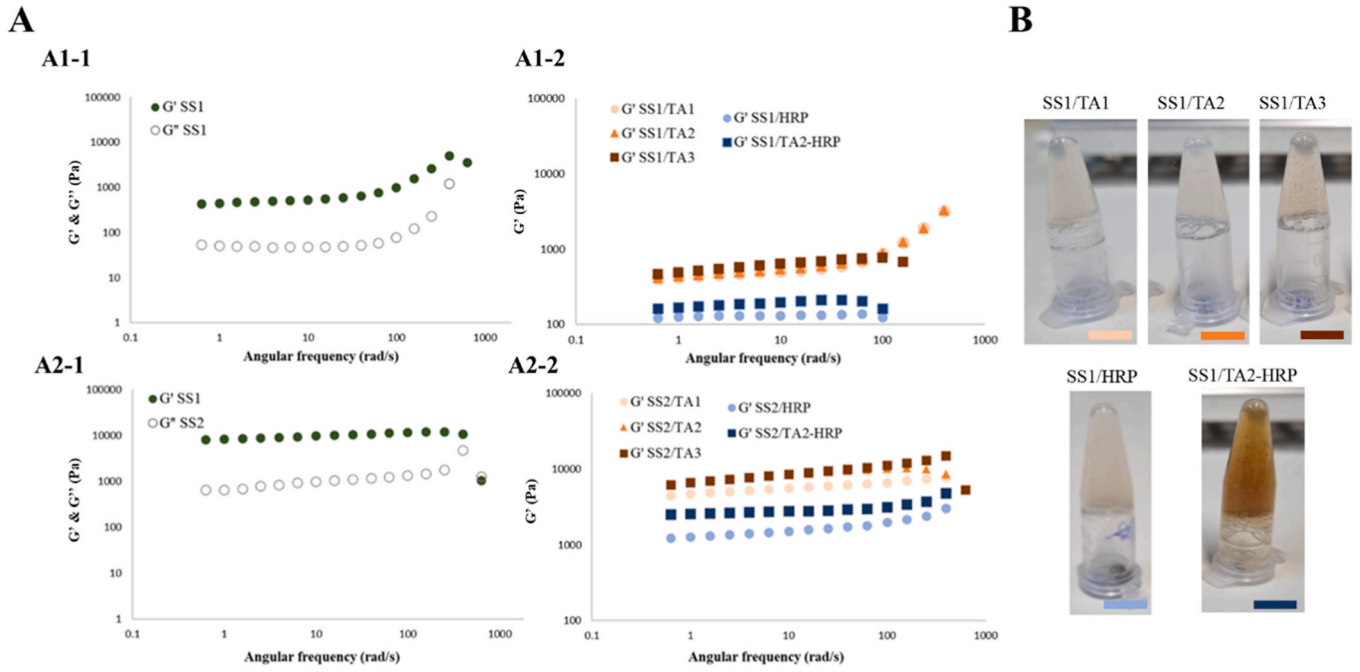

Fig. 2. A) Frequency sweep tests for the different formulations with different SS concentrations: (A1–1) G' and G'' for SS1 (l% wt.); (A2–1) G' and G'' for SS2 (5 % wt.); G' of the different crosslinking systems tested using SS1 (A1–2) and SS2 (A2–2) and B) macroscopic images of the formulations after gelification.

turn would increase crosslinking [67]. However, excessive use of H_2O_2 resulted in H_2O_2-induced cell death, with a delayed gelation process [68, 69].

Regarding the effect of SS concentration on the hydrogels, higher SS amounts led to the formation of hydrogels with higher G' (G' between 100 – 1000 Pa for 2.5 % and 1000–10 000 Pa for 5 %), attributed to intrinsic SS gelation properties. Moreover, the gelation rate becomes higher as the concentration of SS solution increases [70], and a similar trend was observed for both SS concentrations studied (TA3 > TA2 > TA1 > HRP/TA > HRP).

A decrease in viscosity (η) as a function of the applied shear rate was observed, indicating shear-thinning properties for all the tested formulations (Fig. 3 **A1, B1**).

This behavior is characteristic of SS [71] due to molecular entanglement or gelation resulting in shear thinning. This is an important characteristic of hydrogels that can be beneficial in applications that involve extrusion such as injection [18,72].

The largest differences occur up to approximately 1 rad/s (Fig. 3 **A2, B2**). For the SS1 samples, with increasing concentrations of TA, there was an increase in viscosity (at 0.1rad/s with 323, 349, and 557 Pa·s for TA1, TA2, and TA3, respectively). The lowest initial η is attributed to HRP (69 Pa·s), followed by HRP/TA2 (225 Pa·s). The same trend was registered for SS2, with TA conditions exhibiting similar results (TA3–3256 Pa·s > TA1–3170 Pa·s > TA2–2909 Pa·s > SS2/TA2-HRP-1137 Pa·s > SS2-HRP- 566 Pa·s). The flow sweeps are consistent with the findings from the frequency sweeps, confirming the shear-thinning of the different hydrogel formulations. Since TA1, TA2, and TA3 did not yield distinguishable results, TA2 was selected to conduct subsequent tests.

Dynamic shear evaluation was conducted using a three-step flow test to assess SS-based hydrogels potential application in wound healing scenarios (1: initial low shear strain to observe the initial properties of the hydrogel; 2) abrupt increase in shear strain to represent the higher mechanical stresses the hydrogel might encounter during injection into a wound; 3) reduction to the initial shear strain after the high shear strain phase to evaluate the material's ability to recover and stabilize at the wound site.

According to the rheology results, the formulations that exhibited complete recovery after undergoing high shear stress were SS1/HRP, SS2/HRP, and SS2/TA2-HRP. SS2/TA2 was the hydrogel with the least recovery. Regarding formulations with SS1, only HRP-based hydrogels adopted the initial conformation at the end of the three-step flow test. Both SS1/TA2 and SS1/TA2-HRP had a slight decrease in G', G'' (Fig. 4).

Dynamic Shear Rheometric response and mechanical stability are important properties of injectable hydrogels for drug delivery [73]. When hydrogels become less viscous under shear stress, it is easier for them to spread and conform to the contours of the wound site. This ensures that the dressing adheres well to the wound surface. After application, the material should regain higher viscosity, ensuring that it maintains its structure and conforms to the wound site without excessive deformation [74–76]. Recovery profiles can provide insight into how the material responds to compression forces, important where wound dressings may experience compression from external sources, such as clothing or bandages [74,77].

Thus, according to the results, SS-HRP and SS2/TA2-HRP materials are indicated for applications that include initial mechanical forces. On the other hand, SS/TA2 and SS1/TA2-HRP should be used in their final stabilized 3D state and not be subjected to additional applied forces. SS with preserved structural properties, such as gelling capability after dissolution from lyophilized powder, offers potential [18].

3.1.3. *Swelling, retention, and degradation tests*

The swelling profile of the SS-based hydrogels showed maximum water uptake after 1–3h of immersion in H_2O (Fig. 5 A1, B2) and PBS (Fig. 5 A2, B2), and decreased after that period.

For SS1/TA2 the behavior was similar in water and PBS with a maximum uptake of 17–23 %, which after 6 h reached 10–11 %. Different behavior in PBS and H_2O was observed regarding the remaining SS1-based formulations. For SS1/HRP, a stable swelling ratio profile was registered during 6 h in H_2O (from 5 % after 1 h to 2 % after 6 h), and in PBS (from 19 % after 1 h to 11 % after 6 h). SS1/TA2-HRP hydrogels remained stable in H_2O for 3 h (from 2 % after 1 h to 3 % after 3 h). Subsequently, degradation occurred, resulting in a reduced weight during the collection for weighing. In PBS, SS1/TA2-HRP behavior was similar to SS1/HRP from 20 % after 1 h to 9 % after 6 h).

This also occurred for the higher SS concentration (SS2), where the

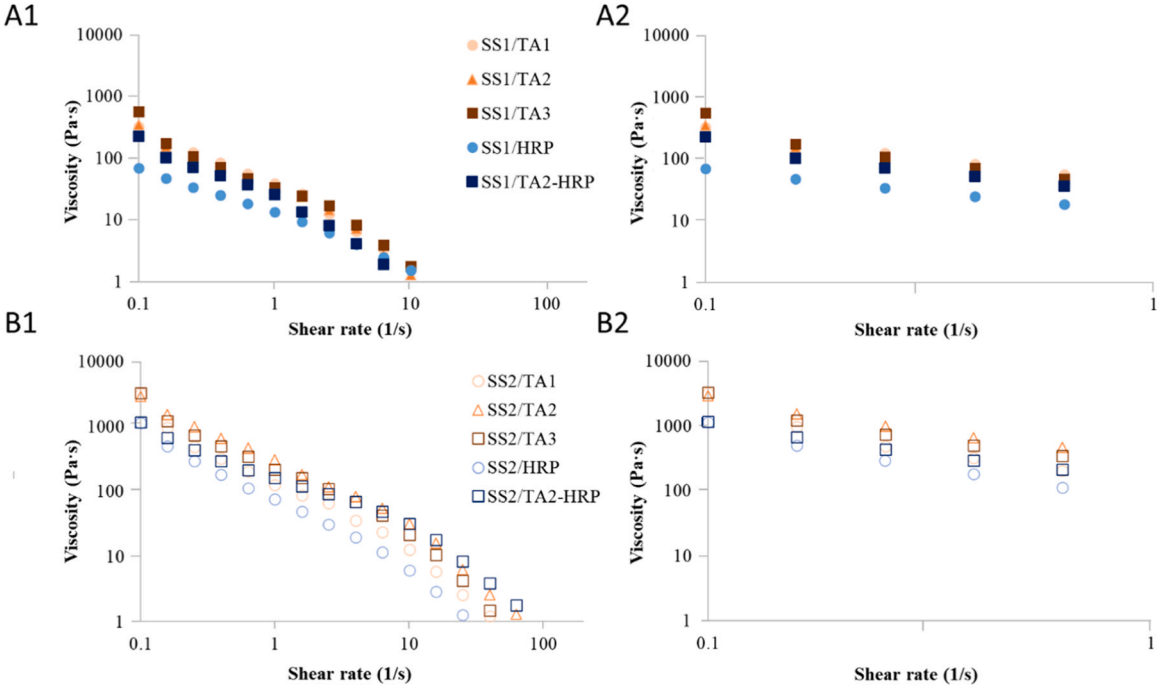

Fig. 3. Flow sweeps for the different SS formulations studied: (A) SS1 (**2.5 %**wt.) and (B) SS2 (**5 %**wt.), from 0.1 to 10 (1/s) (A1, B1) and 0.1–1(1/s) (A2, B2).

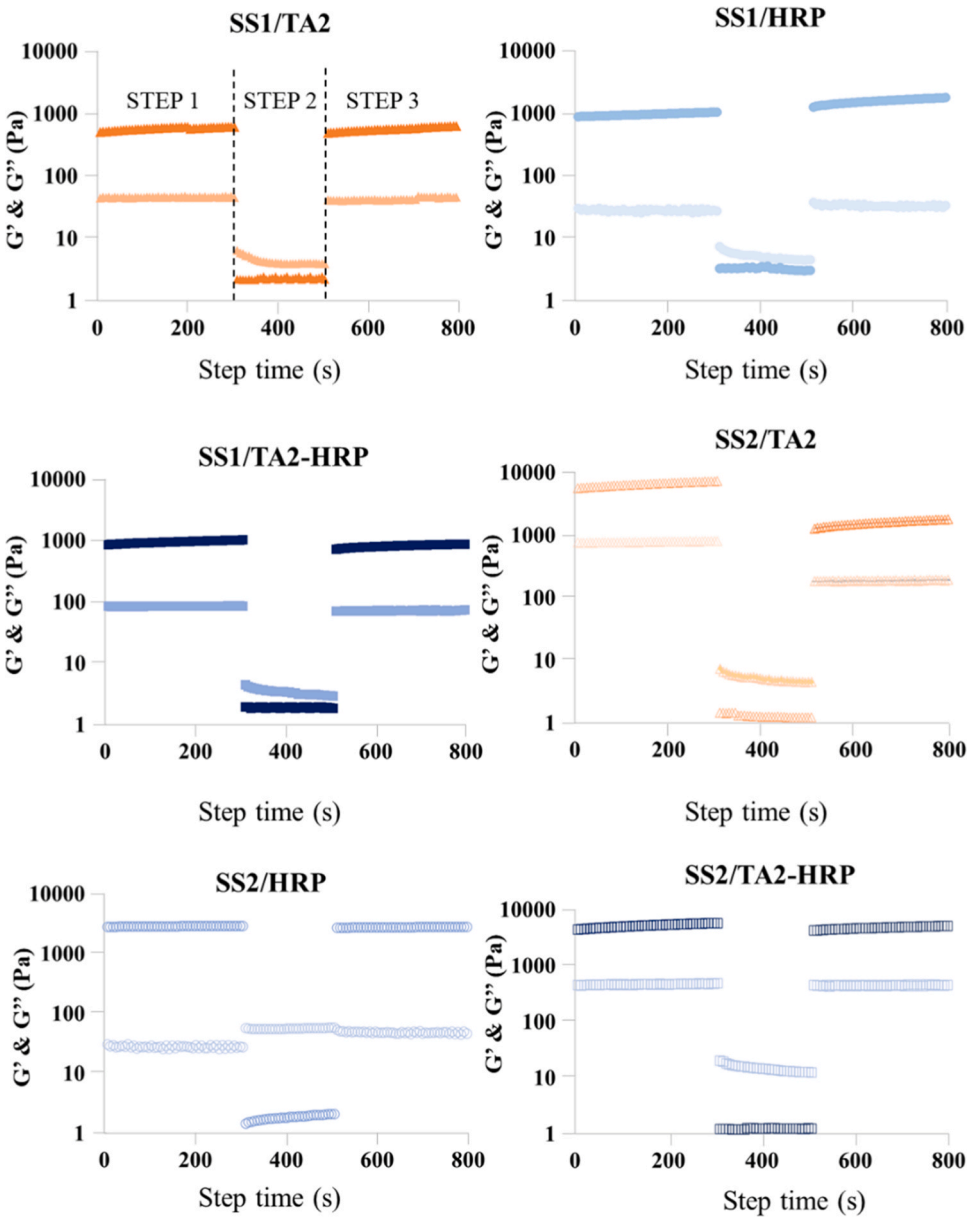

Fig. 4. Recovery profiles of the crosslinked SS1 and SS2 formulations (SS/HRP, SS/TA2, and SS/TA2-HRP), using a three-step flow test: 1) 1 % shear strain at 1 Hz for 5 min, B) 1000 % shear strain for 3.33 min and C) 1 % at 1 Hz for 5 min.

swelling ratios in H_2O (ranging from 2 % to 7 %) at the end of 6 h were lower than those obtained with immersion in PBS (ranging from 9 % to 14 %). Furthermore, the profiles in PBS were similar between the different experimental conditions, and the maximum swelling occurred after 1 h (reaching 24 %, 22 %, and 18 % for SS2/TA2, SS2/HRP, and SS2/TA2-HRP, respectively).

In PBS, the retention capacity after 30 h was higher for SS2-based conditions and remained constant (between 24 and 30 h). The SS1 materials, which have lower G′ and are therefore less rigid, showed a higher loss of adsorbed PBS (Fig. 5 **A3, B3**).

The swelling capability and fluid interactions of the hydrogels, such as the SS2, are crucial when considering applications as wound dressing [21]. Fluid absorption is essential to manage moisture balance [78]. On the other hand, for wounds with eschar, characterized by being dry, extra moisture is required and could be provided by the SS1-based materials. The size of the wound also plays a crucial role in selecting the most adequate material. For deeper wounds, a stable 3D hydrogel with sufficient G' such as SS2 can be used to fill the affected area and promote healing and regeneration [78].

No significant degradation occurred for SS2/TA2-HRP hydrogels when immersed in protease XIV (Fig. 6). However, the SS2/TA2 and SS2/HRP hydrogels underwent 4 and 11 % degradation (mass loss ratio), respectively, after 50 h. Degradation rates were around 8 % for SS1/TA2, 10 % for SS1/HRP, and 7 % for SS1/TA2-HRP after 50 h of incubation in the protease.

These results indicate that SS-HRP hydrogels had good stability in PBS (Figs. 6 **A,B**), which decreased with the concentration of SS. Hydrogels containing TA and HRP (TA2-HRP) degraded similarly to those containing only HRP, indicating that no synergistic crosslinking effect was achieved. When added alone to the SS formulation, TA did not contribute to stabilizing the structure and therefore the degradation rate was higher. In the presence of protease (Figs. 6 **C,D**), SS-HRP hydrogels degraded faster due to proteolytic degradation as previously described [21,73]. Interestingly, the results showed that in the presence of TA, the proteolytic activity decreased, contributing to overall stabilization.

TA is recognized for its polyphenolic structure, featuring numerous

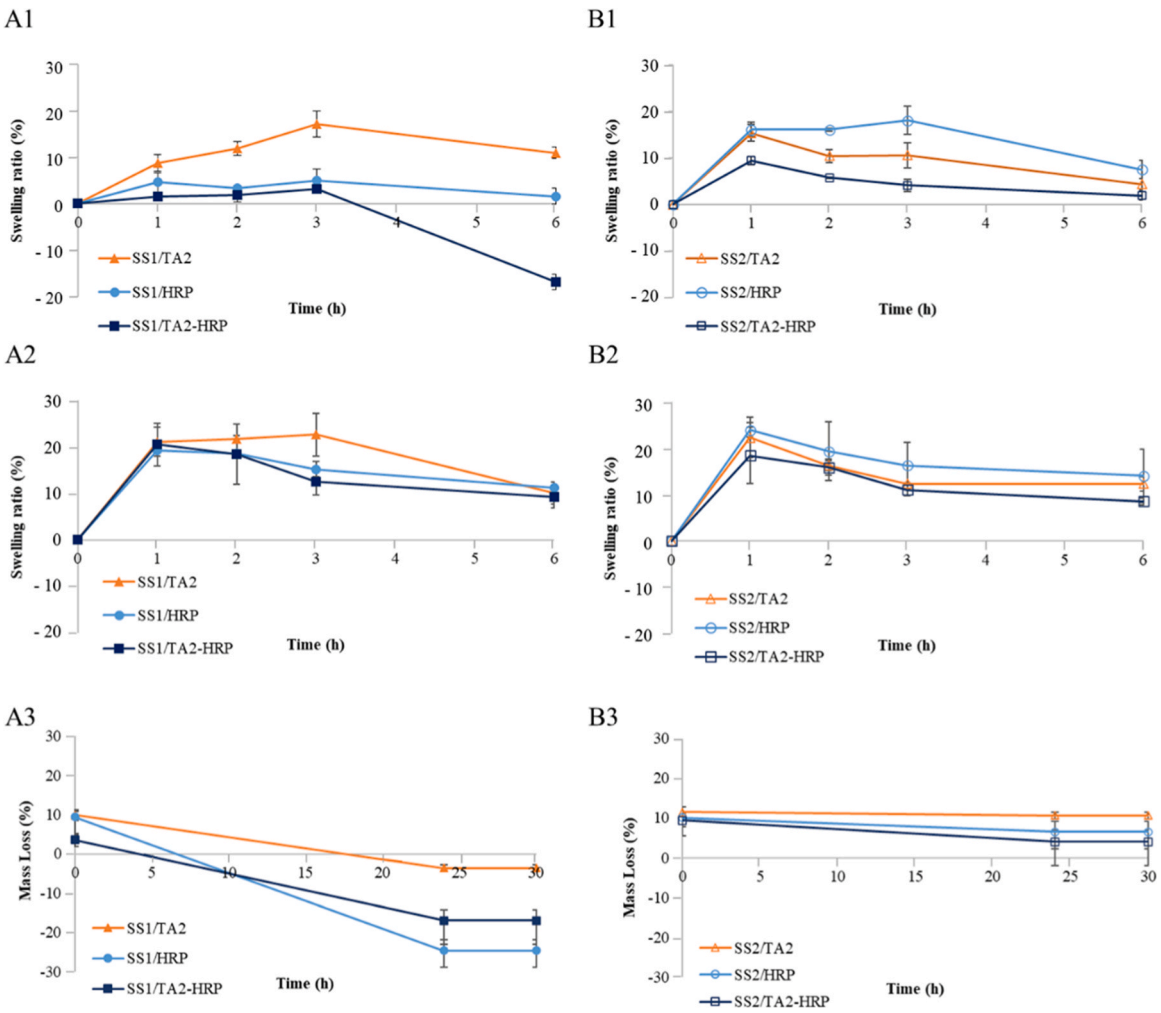

Fig. 5. Material testing of (A) SS1 (**2.5 %**wt.) and (B) SS2 (5 % wt.): swelling ratio profiles in ultrapure water (1) and PBS (2) and retention ratio profiles (3) that represent the ability of the SS-hydrogels to maintain adsorbed PBS after 24 h of swelling (time point 0).

hydroxyl groups capable of interacting with proteins and enzymes [79]. In the context of enzymatic degradation within the hydrogel, these hydroxyl groups serve as multiple sites for interactions with both the protease and the hydrogel network. TA's capacity to form hydrogen bonds and undergo complexation with proteins may lead to molecular complexes or altered structural arrangements at the hydrogel-protease interface [77,80]. Furthermore, TA's metal-chelating ability has the potential to modulate enzymatic activity, possibly by influencing the catalytic metal cofactors essential for protease function [81]. As a result, the interaction of TA with the protease could potentially restrict access to the hydrogel network, thereby limiting enzymatic degradation.

3.1.4. Antioxidant behavior

Antioxidant-rich hydrogel systems have potential in the field of wound tissue repair. Injuries resulting from trauma, surgical procedures, or chronic conditions introduce the body to a state of oxidative stress [34,82,83]. This condition is marked by the accumulation of harmful reactive oxygen species (ROS) at the wound site. These ROS can exacerbate tissue damage and hinder the innate healing processes, culminating in complications like delayed wound closure, heightened inflammation, and elevated susceptibility to infections. Antioxidant hydrogels play a crucial role in mitigating these adverse effects by neutralizing ROS, thereby creating a microenvironment that promotes ideal conditions for wound healing [84,85].

The scavenging effect, which refers to the ability to neutralize ROS and prevent their harmful effects, was evaluated for the different SS1 formulations. According to the DPPH test (Fig. 7), the increase in SS concentration resulted in the absence of a scavenging effect [32,86,87].

Reduced accessibility can explain this phenomenon: SS molecules may become densely packed, making it challenging for free radical access. Increasing SS concentration decreased gelling time and resulted in denser hydrogels [86] with a higher G' and resistance to degradation as verified. The experimental condition with the most scavenging effect was SS1/TA2 (after incubation for 30 min and 1 h). This effect increased over time (from 1 to 7 days). On the other hand, SS1/HRP extracts showed high scavenging effects, particularly those at 3 and 7 days.

SS1/TA2 antioxidant behavior can be attributed to the presence of both SS and TA which contain antioxidant properties. The scavenging effect of SS1/HRP can be attributed to SS, and the crosslinking mechanism used may enhance its ability to scavenge free radicals [32,87]. The time-dependent changes indicate that the materials could maintain their antioxidant properties over time.

3.2. In vitro biological assessment

3.2.1. Indirect contact assay

Indirect tests to evaluate the cytotoxicity of the formulations demonstrated that all studied hydrogels were cytocompatible, according to the ISO10993–5 standard (Fig. 8).

The SS1/HRP formulation resulted in higher cell viability when compared with the TA formulation. Although some earlier results mentioned potential immunogenicity reactions, recent data clarify that

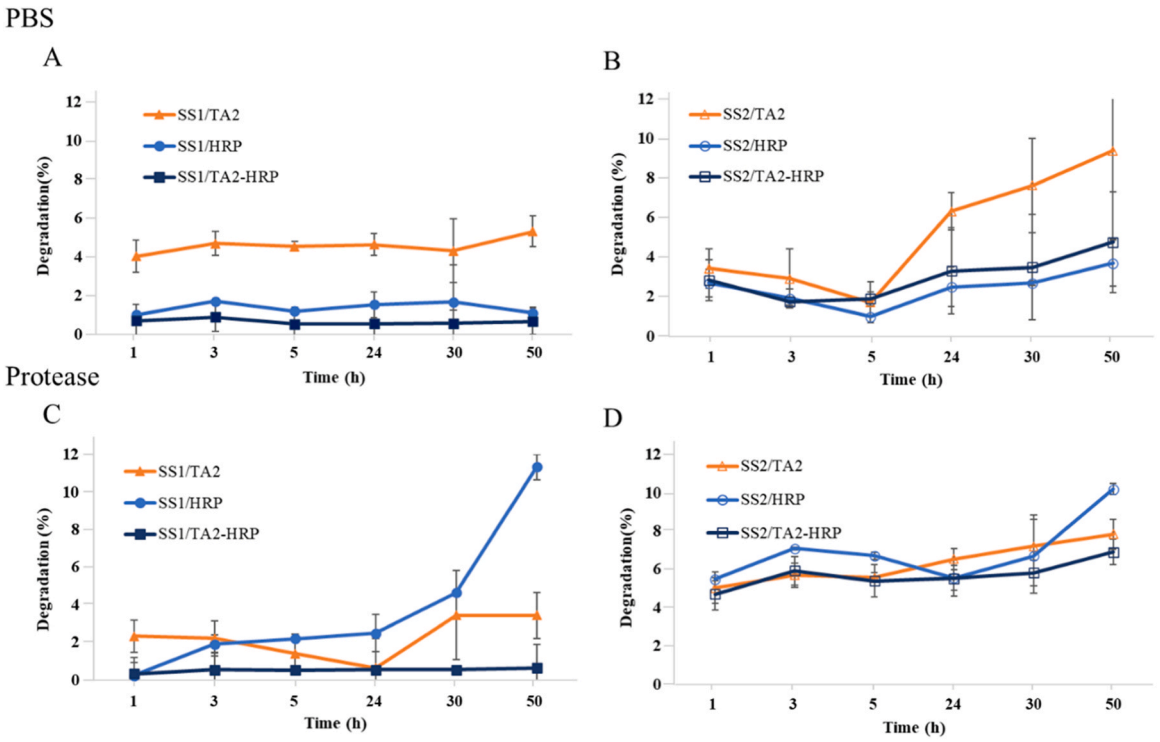

Fig. 6. Degradation profile as a representation of mass loss ratio (%) up to 50 h in PBS (A: SS1, B: SS2) and protease XIV (C: SS2, D: SS2).

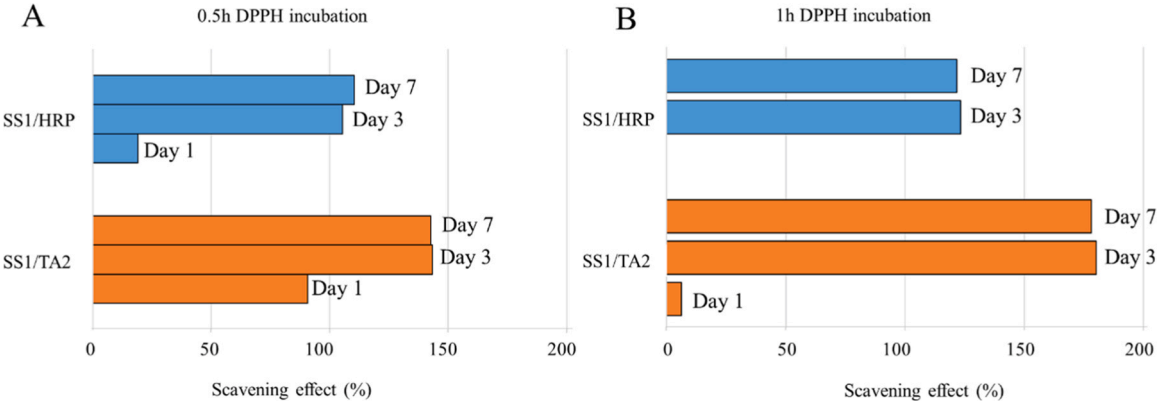

Fig. 7. Scavenging effect (%) of the extracts collected after 1, 3, and 7 days of incubation in the SS-based hydrogel formulations for A) 0.5 h and B) 1 h after initial incubation with the DPPH reagent.

with suitable extraction and processing methodologies, sericin promotes cell adhesion and proliferation [88,89]. In our recent study, we demonstrated that the methodology adopted does not affect cell migration of HDFs, as shown in our previous work after performing a scratch test and visualizing cell migration over time [15]. However, the development of new crosslinking systems can affect these properties, and it is thus fundamental to assess cytotoxicity.

3.2.2. *Direct contact assay*

The results from the direct contact test indicated a general increase in metabolic activity over the 7-day cell culture period for the studied formulations. However, it is noteworthy that, except for SS2/TA2 and SS2/TA2-HRP, no significant differences were observed between the different time points. This suggests a consistent trend of metabolic activity enhancement over time for most formulations, while SS2/TA2 and SS2/TA2-HRP exhibited distinct behavior, which suggests a combined effect of SS2 and TA2. Differences between 1 and 7 days were greater for SS1/TA2 (***) and SS1/HRP and SS2/HRP (****), than for SS1/TA2-HRP (*) (Fig. 9).

Recently, we have successfully applied the SS/HRP/H_2O_2 hydrogel system in an *in vivo* diabetic wound model, validating the feasibility of the hydrogel in an *in-situ* approach [21]. This finding aligns with the results of this study for the SS/HRP system, where enhanced fibroblast proliferation was observed compared to other SS hydrogel formulations. Moreover, by increasing the SS hydrogel concentration from 2.5 % to 5 % (SS1 to SS2) an increase in cell proliferation was observed. This effect is likely related to an increase in hydrogel stiffness (higher G' for SS2 with rheological testing) and an increase in anchorage sites for the cells to adhere, migrate, and proliferate. The conditions containing TA2 presented lower metabolic activity compared to those where only HRP was used as the crosslinking agent. This result is with following the indirect contact assays where a reduction of cell viability was also observed in the presence of TA. The possible release of unbonded TA molecules in both SS and SS/HRP hydrogels might induce a decrease in

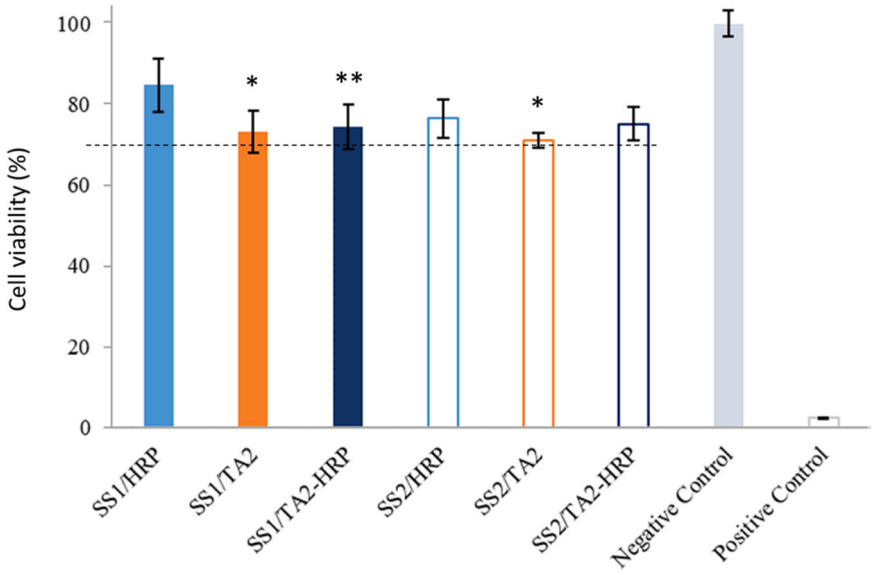

Fig. 8. Cell viability of the formulations studied after 24 h of cell culture (significance level of *p < 0.05, **p < 0.01in relation to SS1/HRP, by applying One-way ANOVA followed by Tukey's method). Control 2D HDFs were used as a positive control to calculate cell viability and cells incubated with DMSO were used as a negative control.

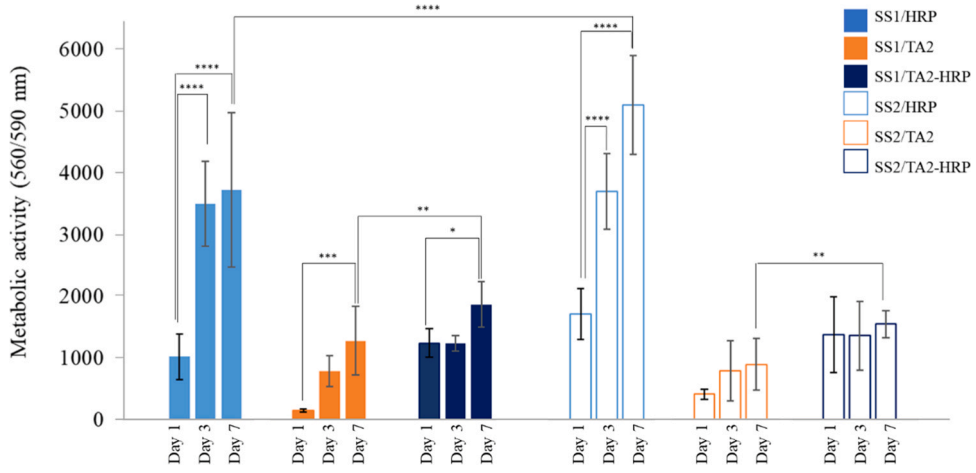

Fig. 9. Metabolic activity of cells cultured in direct contact with different SS-based hydrogel formulations for 1,3 and 7 days (significance level of *p < 0.05, **p < 0.01, ***p < 0.001, ****p < 0.0001 by applying One-way ANOVA followed by Tukey's method).

the cell viability for both indirect and direct contact assays. In recent studies, TA-based hydrogels have been applied to induce cell death and oxidative stress of different cell types such as human liver hepatocellular carcinoma cells [90] and A549 human lung cancer [91]. This might open a new application route for the SS/TA-based systems.

The significant differences in metabolic activity were registered between the first and last day of cell culture, being more pronounced for SS/HRP, followed by SS1/TA2 and SS1/TA2-HRP. For the tested conditions, an overall trend between the added crosslinker and the ability to stimulate cell metabolic activity was registered: HRP > TA2-HRP> TA2. Since comparable cell metabolic activity behavior was obtained in both SS1 and SS2 formulations (with more statistical difference over time registered for SS1), SS1 was chosen to perform DNA quantification, Live/Dead assay, and Confocal imaging (Fig. 10) [84,85].

Overall, the DNA content of SS1/HRP, SS1/TA2, and SS1/TA2-HRP supported the cell metabolic activity results (Fig. 10 **A**): SS1/HRP had a significant increase in DNA content after 1 week of cell culture, while no significant differences were observed for SS1/TA2 and SS1/TA2-HRP formulations. The presence of viable cells in the SS1 hydrogels was analyzed using the live/dead assay (Fig. 10 **B**). The results showed that cells remained viable for all tested conditions. After 24 h, cells were visible on the top surface of all hydrogel constructs, presenting a round morphology (visible through the green staining for day 1). No dead cells were observed in the live/dead imaging, which demonstrated good viability for the HDFs seeded on top of the hydrogels (cell seeding efficiency of approximately 90 % [32]). After 7 days, cells spontaneously migrated to the interior of the hydrogels, and it was necessary to perform a cross-section to visualize them (**SI-4**).

The infiltrated cells in the different 3D structures maintained their viability, which correlates with the AlamarBlue results (Fig. 10). Moreover, the number of cells for SS1/HRP formulations increased over time. The cell controls are included in **SI-5** and the results were further corroborated by confocal images (Fig. 10 **C**).

3.2.3. *Cell embedding*

SS1 formulations were also selected to embed cells within the hydrogel matrices, where the cell pellet was directly mixed with the crosslinked SS-formulation (**SI-6**). The HDFs (5×10^5 cells/gel) survived

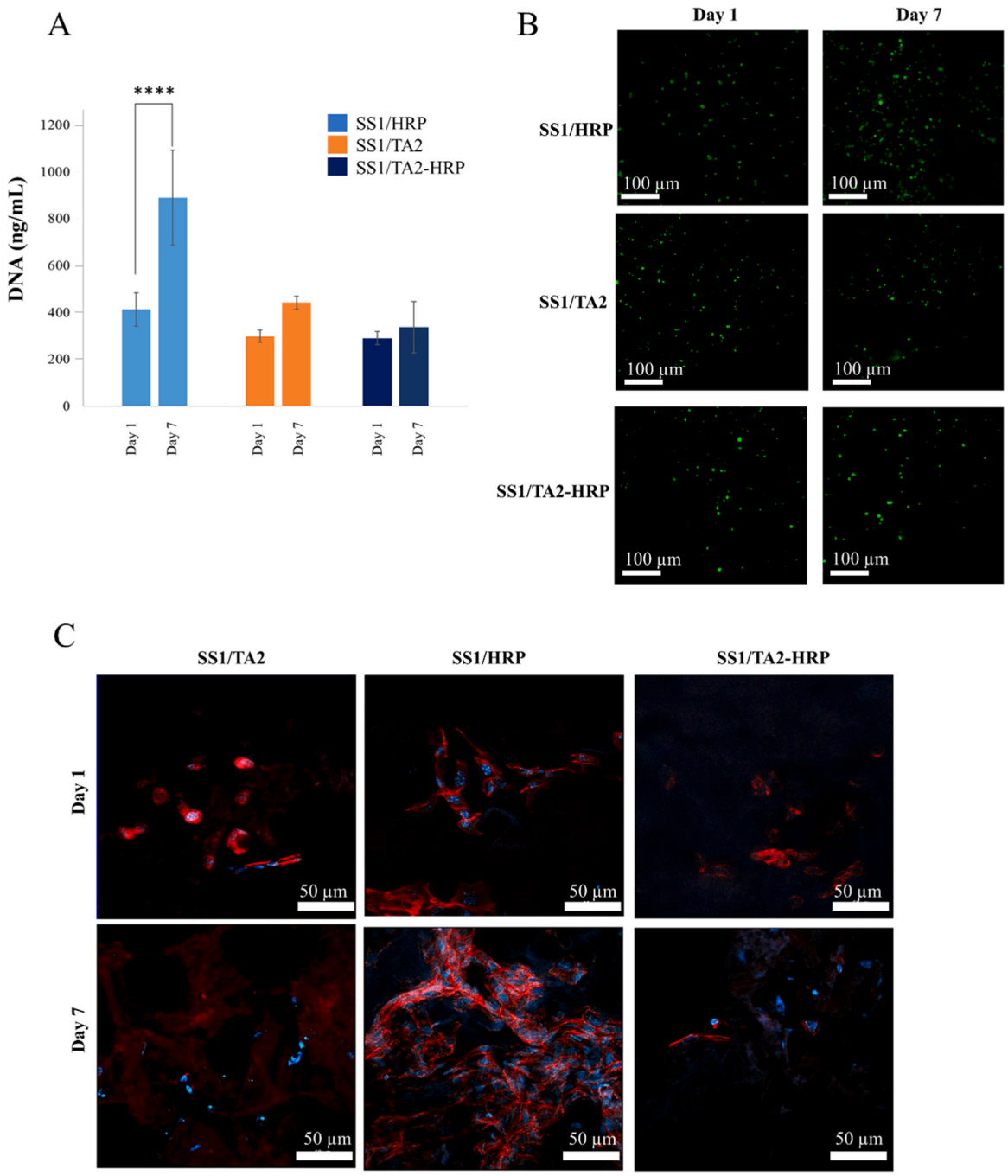

Fig. 10. A) DNA quantification for SS1-based formulations and B) Live/Dead images (Magnification 10 ×), and C) confocal images (nucleus and cytoskeleton). (significance level of ****$p < 0.0001$ by applying One-way ANOVA followed by Tukey's method).

the encapsulation process (Fig. 11 **A**). Furthermore, in the SS1/HRP condition, metabolic activity increased over time. Moreover, on day 7 the HDFs exhibited a round-like morphology (also visible in Live/Dead assay after cell seeding), while on day 14 the cells evolved to a stretched cytoskeleton (Fig. 11 **B**). According to the recovery profiles, SS1/HRP exhibited the best rheological recovery capacity which may relate to the mechanical stresses associated with cell interactions [92].

In contrast, cell metabolic activity of SS1/TA2 and SS1/TA2-HRP formulations decreased over time, indicating that these formulations were not suited for encapsulation (Fig. 11 **A**).

At a lower cell density (1×10^5 cells/gel), the metabolic activity of the fibroblasts was lower when compared to the tests with higher cell density. Furthermore, growth within the hydrogel remained stagnant (**SI-7**). Low cell densities may limit cell-cell communication and cooperative behavior s including paracrine signaling that are essential for cell survival and function [93].

The formulation that allowed the preservation of metabolic activity (SS1/HRP) was compared with an SF hydrogel (SF1/HRP) based on previous work [94]. Despite being a material used in skin-TE, the application of SF for cell encapsulation is associated with inhibition of cell growth over time as it does not have the peptide motifs for cell adhesion [95,96]. For this reason, the cell suspension was added to a phenol red-free and serum-free DMEM/F12 media prior to encapsulation to include comparison with a control [96]. According to the results, SS results in greater cell activity after 7 days of cell culture (**SI-8**).

Regarding mechanical properties required for cell incorporation,

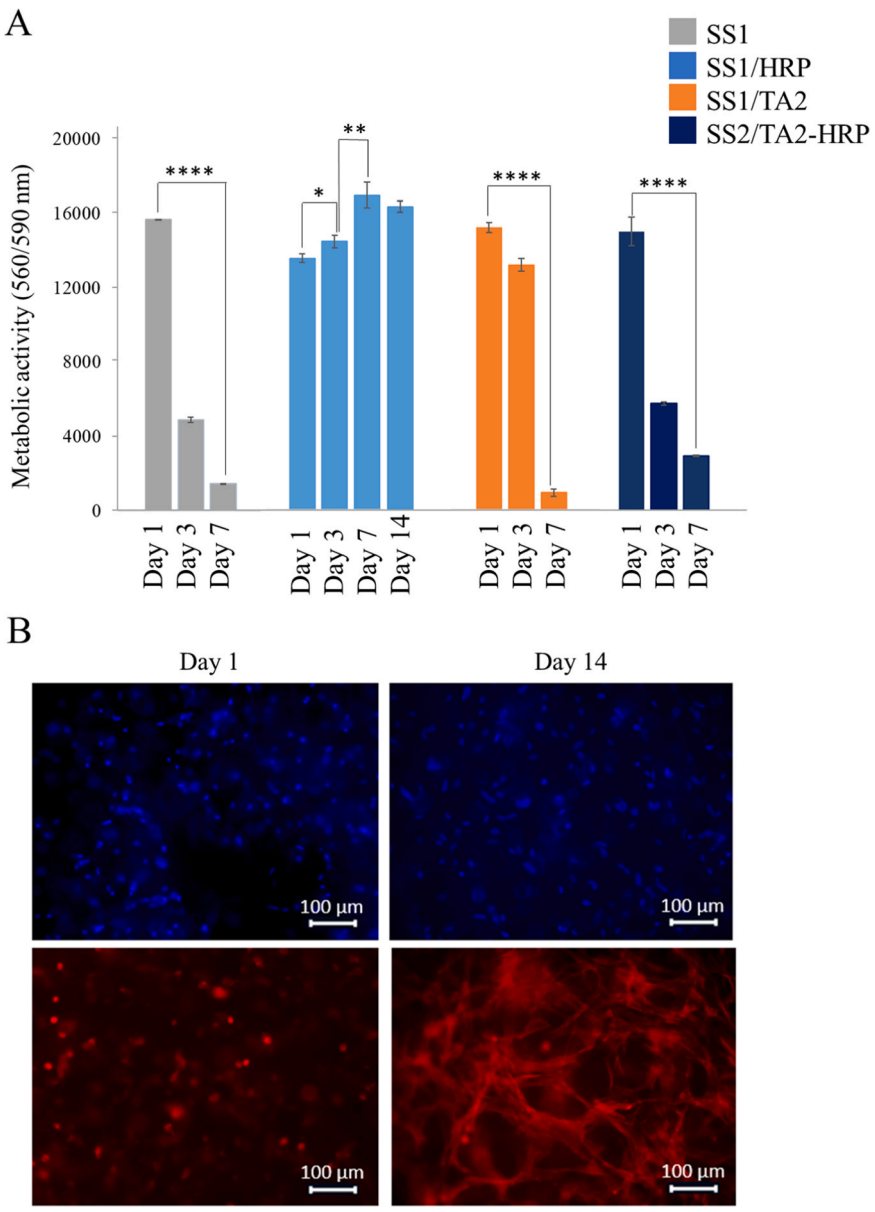

Fig. 11. (A) Metabolic activity for the cell-embedded SS1-based hydrogel formulations, after 1, 3, and 7 days of culture and 14 (for SS1/HRP) (significance level of *$p < 0.05$, **$p < 0.01$, ****$p < 0.0001$ by applying 2-way ANOVA followed by Turkey's method), (B) Z-stack Immunostaining images after 1 and 14 days of cell culture (Phalloidin, DAPI).

fibrous proteins such as SF typically exhibit enhanced strength due to their β-sheet-rich structure [14]. This mechanical advantage is reflected in reported G′ values ranging from 100 to 10,000 Pa for SF hydrogels prepared at 1–5 wt%, depending on crosslinking conditions and formulation [96,97]. In the present study, SS-based hydrogels display G′ values of approximately 400–600 Pa, which, while lower, fall within the range suitable for soft tissue engineering applications. Mechanical tuning of the SS system remains feasible through polymer concentration adjustment and integration of reinforcing agents [50].

Gelatin-based hydrogels typically require chemical crosslinking (e.g., with genipin or enzymatic systems) to achieve stable mechanical properties, with G′ values generally between 0.5 and 5 kPa [98]. Although mechanically stronger than the SS system, gelatin's thermosensitivity and low inherent stiffness may limit its standalone use. Similarly, collagen hydrogels show moderate stiffness (1–10 kPa) and good biocompatibility, but rapid enzymatic degradation often compromises long-term structural integrity [99]. Albumin-based hydrogels, particularly those using BSA, exhibit tunable mechanics with G′ values ranging from a few Pa to ~5000 Pa, depending on ethanol- or enzyme-induced gelation methods. Some BSA hydrogels show self-healing behavior and notable antimicrobial activity [100].

Self-assembling peptide-based systems offer an alternative strategy, with mechanical properties highly dependent on molecular design. Escuder et al. describe supramolecular hydrogels based on low molecular weight peptides with G′ values below 1 kPa, optimized for responsiveness and minimalistic design [101]. Adler-Abramovich and co-workers explored alginate-FmocFF composite hydrogels with storage moduli approaching 10 kPa and demonstrated osteoinductive potential and thixotropy—useful for injectable applications [102]. Bitton et al. showed that peptide-functionalized alginate hydrogels can reach G′ values significantly higher than non-modified controls due to enhanced peptide junction zones, supporting fine control of mechanical cues in artificial ECM design [103].

Shuguang Zhang's work with RADA16 self-assembling peptide hydrogels emphasizes long-term 3D neural culture, with stiffnesses in the low-kPa range and enhanced cell differentiation when

functionalized with adhesion motifs [104]. Similarly, Ulyana Shimanovich et al. developed enzymatically active microgels based on amyloid fibrils that are stable and porous, although quantitative mechanical data were not the focus of that study [105]. Kaplan et al. demonstrated that enzymatically crosslinked SF/gelatin composite hydrogels can be fine-tuned for stiffness and degradation via tyramine conjugation, reaching moduli in the mid-kPa range suitable for cell encapsulation [96].

Thus, while the SS hydrogels reported here exhibit relatively lower storage moduli compared to some of the above systems, they remain within a biomechanically relevant range for soft tissue applications. Furthermore, their simplicity of formulation, biodegradability, antioxidant potential and cytocompatibility make them a viable alternative or complementary system within the broader class of protein- and peptide-based hydrogels.

Other cell embedding systems for wound healing have been reported to require 0.5 – 2 × 10^6 cells/mL to promote the adhesion and proliferation of different cells. For instance, previous studies reported Human Adipose-derived stem cells (ADSCs) added to a GelMA-methacrylate hyaluronic acid (HAMA) (0.5 × 10^6–2 × 10^6 cells/mL) [106] and to Chitosan-Gelatin (1 × 10^6 cells/mL) [107] hydrogels. These cell densities supported cell proliferation and enhanced vascularization (CAM assay demonstrated newly growing blood vessels). Mice bone marrow mesenchymal stem cells (BMSC) were added to a Poly NIPAM- poly (amidoamine) hydrogel (1 × 10^6 cells/mL) resulting in a sustained release of ADSC that suppressed inflammation and accelerated wound contraction, granulation tissue formation when used in a diabetic rat wound model [108].

3.3. Potential applications and current limitations

Overall, the formulations studies have different properties that can be explored according to the final application (**SI-9**). SS1/HRP demonstrates excellent potential for 3D bioprinting due to its shear-thinning behavior, which facilitates smooth extrusion, and its rapid recovery, which helps maintain the printed structure and prevent unwanted spreading [50]. In addition, its ability to support cell metabolic activity—likely linked to its higher amorphous content and improved nutrient and oxygen diffusion—promotes uniform cell distribution and proliferation within the 3D matrix [109]. These features open new possibilities for developing natural, patient-specific functional matrices [78,110, 111].

In contrast, while SS1/TA2 and SS1/TA2-HRP also promote cell activity over 7 days of culture, they appear better suited for applications requiring softer materials. SS1/TA2 and SS1/TA2-HRP formulations are ideal for developing 2D films for superficial wound treatment [112] or as coatings for medical implants, where their mild effect on cell viability, along with antioxidant properties that prevent oxidative stress and enhance collagen synthesis [113–115], contribute to improved tissue integration without provoking excessive cell adhesion that could lead to fibrous capsule formation or scarring. Moreover, the high stability of SS1/TA2-HRP in the presence of proteases [116] further supports its potential in such applications. Similar hydrogel-based approaches have been used to immobilize bioactive enzymes and suppress biochemical activity in pathological conditions, demonstrating the therapeutic versatility of supramolecular gels [117].

Hydrogels formulated with a higher sericin concentration (SS2) exhibit greater stiffness and retention capacity compared to SS1. These properties make SS2-based hydrogels suitable for maintaining wound moisture and for constructing larger, structurally robust 3D scaffolds aimed at deep wound filling [78]. Although SS2/TA2 and SS2/TA2-HRP do not stimulate cellular metabolic activity, their unique characteristics may be exploited for applications that aim to inhibit cancer cell proliferation [90,91] or even serve as nutrient media to facilitate long-distance cell transport [118,119]. Long-term cell culture in these systems is also crucial for developing drug testing and disease modeling platforms [120]. Additionally, SS2/HRP, with its shear-thinning and thixotropic behavior, shows promise for in situ applications, as initially proposed in previous work [32], and for treating deeper wounds to promote cell proliferation. Additionally, other studies have demonstrated the potential of sulfated bacterial cellulose/gelatin scaffolds for hepatocyte culture in 3D, reinforcing the broader applicability of biocompatible hydrogel matrices in long-term *in vitro* tissue models [121].

Future directions in this area could include the incorporation of nanoparticles and growth factors to further enhance cell adhesion and proliferation [122], together with testing in advanced *in vivo* models.

4. Conclusions

The current research lays the foundation for the development of new SS-based hydrogels by proposing a protocol that utilizes a sterile and soluble SS powder to produce enzymatically crosslinked hydrogels with tunable properties. The synergistic effects of TA on the physicochemical and rheological properties of SS and SS/HRP, as well as biological performance of 3D SS hydrogels in an *in vitro* HDF model, have been demonstrated. SS1/HRP hydrogel were explored for the first time as a supportive environment for promoting cell viability and function after embedding. Additionally, due to its shear-thinning properties, cell maintenance, and amorphous components aiding nutrient diffusion, these hydrogels show potential as a bioink for 3D bioprinting. Stiffer SS2 hydrogels offer high fluid retention for wound care, and SS2/HRP are more suitable for *in situ* applications, supporting stable 3D hydrogel production for deeper wounds.

On the other hand, TA-based formulations (SS1/TA2 and SS1/TA2-HRP) are more suited as 2D films and coatings due to their softer nature and mild effect on cell viability. While the current biological evaluation confirms the general cytocompatibility and bioactivity of the developed hydrogels, further targeted studies will be required to assess their performance in specific tissue engineering contexts and under physiologically relevant conditions. The present SS-hydrogels can serve as a platform for the development of new biomaterials for skin-TE, offering a range of properties tailored to specific applications and outcomes. Overall, this research provides the starting point for future developments, opening diverse possibilities for wound healing and further TE applications.

CRediT authorship contribution statement

Viviana Ribeiro: Writing – review & editing, Methodology, Investigation. **Anabela Veiga:** Writing – review & editing, Writing – original draft, Validation, Methodology, Investigation, Formal analysis, Data curation, Conceptualization. **Maria Rosa Aguilar:** Writing – review & editing, Validation, Supervision, Resources, Methodology. **Rosa Ana Ramírez-Jiménez:** Writing – review & editing, Methodology, Investigation, Formal analysis, Conceptualization. **Ana L. Oliveira:** Writing – review & editing, Writing – original draft, Validation, Supervision, Resources, Methodology, Investigation, Funding acquisition, Formal analysis, Conceptualization. **Luis Rojo:** Writing – review & editing, Writing – original draft, Visualization, Validation, Supervision, Resources, Methodology, Investigation, Formal analysis, Data curation, Conceptualization.

Declaration of Competing Interest

The authors declare that they have no known competing financial interests or personal relationships that could have appeared to influence the work reported in this paper.

Acknowledgments

This work was financially supported by: National Funds through FCT

(Foundation for Science and Technology) under the project UIDB/50016/2020 of the Centre for Biotechnology and Fine Chemistry - CBQF; by LA/P/0045/2020 (ALiCE), UIDB/00511/2020 and UIDP/00511/2020 (LEPABE), funded by national funds through FCT/MCTES (PIDDAC); and IBEROS+ (0072_IBEROS_MAIS_1_E) - Instituto de Biofabricación en Red para El Envejecimiento Saludable, funded by "Interreg VI A España – Portugal (POCTEP) 2021–2027. A. Veiga gratefully acknowledges doctoral scholarship [2020.08683.BD] from FCT and ERASMUS + mobility scholarship from the Faculty of biotechnology-Portuguese catholic University (ESB-UCP). MRA and LR are members of Technological Interdisciplinary Platform SUSPLAST+ and were supported by MICINN PID2020–114086RB-100, PID2023–149301OB-I00 funded by MICIU/AEI (DOI: 10.13039/501100011033) and by ERDF/EU and Autonomous Community of Madrid, Spain, grant S2022/BMD-7406 and by CIBER-BBN (Spain) – Consorcio Centro de Investigación Biomédica en Red (Ref. CB06/01/0013). VR acknowledge the Individual Junior Research contract 2023.07374.CEECIND/CP2855/CT0006 attributed by FCT.

Appendix A. Supporting information

Supplementary data associated with this article can be found in the online version at doi:10.1016/j.colsurfb.2025.114916.

Data availability

Data will be made available on request.

References

[1] E. Troy, M.A. Tilbury, A.M. Power, J.G. Wall, Nature-based biomaterials and their application in biomedicine, Polymers 13 (19) (2021) 3321, https://doi.org/10.3390/polym13193321.
[2] J.R. Yu, et al., Current and future perspectives on skin tissue engineering: key features of biomedical research, translational assessment, and clinical application, Adv. Health Mater. 8 (5) (2019), https://doi.org/10.1002/adhm.201801471.
[3] T. Shi, et al., Naturally derived dual dynamic crosslinked multifunctional hydrogel for diabetic wound healing, Compos B Eng. 257 (2023) 110687, https://doi.org/10.1016/j.compositesb.2023.110687.
[4] A. Veiga, F. Castro, F. Rocha, A. Oliveira, Protein-based hydroxyapatite materials: tuning composition towards biomedical applications, ACS Appl. Bio Mater. (2020), https://doi.org/10.1021/acsabm.0c00140 p. acsabm.0c00140, Apr.
[5] S. Cheng, et al., A motion-responsive injectable lubricative hydrogel for efficient Achilles tendon adhesion prevention, Mater. Today Bio 30 (2025), https://doi.org/10.1016/j.mtbio.2025.101458.
[6] P. Aramwit, T. Siritientong, T. Srichana, Potential applications of silk sericin, a natural protein from textile industry by-products, Waste Manag. Res. 30 (3) (2012) 217–224, https://doi.org/10.1177/0734242X11404733.
[7] K. Tsubouchi, Y. Igarashi, Y. Takasu, H. Yamada, Sericin enhances attachment of cultured human skin fibroblasts, Biosci. Biotechnol. Biochem 69 (2) (2005) 403–405, https://doi.org/10.1271/bbb.69.403.
[8] A. Veiga, F. Castro, F. Rocha, A. Oliveira, Silk-based microcarriers: current developments and future perspectives, IET Nanobiotechnol 14 (8) (2020) 645–653, https://doi.org/10.1049/iet-nbt.2020.0058.
[9] P. Aramwit, S. Kanokpanont, T. Nakpheng, T. Srichana, The effect of sericin from various extraction methods on cell viability and collagen production, Int J. Mol. Sci. 11 (5) (2010) 2200–2211, https://doi.org/10.3390/ijms11052200.
[10] L. Liu, et al., Systematic evaluation of sericin protein as a substitute for fetal bovine serum in cell culture, Sci. Rep. 6 (1) (2016) 31516, https://doi.org/10.1038/srep31516.
[11] J.P. Kumar, B.B. Mandal, Antioxidant potential of mulberry and non-mulberry silk sericin and its implications in biomedicine, Free Radic. Biol. Med 108 (2017) 803–818, https://doi.org/10.1016/j.freeradbiomed.2017.05.002 (no. February).
[12] A. Veiga, F. Castro, C.C. Reis, A. Sousa, A.L. Oliveira, F. Rocha, Hydroxyapatite/sericin composites: A simple synthesis route under near-physiological conditions of temperature and pH and preliminary study of the effect of sericin on the biomineralization process, Mater. Sci. Eng. C 108 (2020) 110400, https://doi.org/10.1016/j.msec.2019.110400.
[13] A. Veiga, O. Foster, D.L. Kaplan, A.L. Oliveira, Expanding the boundaries of silk sericin biomaterials in biomedical applications, J. Mater. Chem. B 12 (29) (2024) 7020–7040, https://doi.org/10.1039/D4TB00386A.
[14] J.K. Sahoo, O. Hasturk, T. Falcucci, D.L. Kaplan, Silk chemistry and biomedical material designs, Nat. Res. (2023), https://doi.org/10.1038/s41570-023-00486-x.
[15] A. Veiga, et al., Innovative processing and sterilization techniques to unlock the potential of silk sericin for biomedical applications, Gels 11 (2) (2025) 114, https://doi.org/10.3390/gels11020114.
[16] Z. Wang, et al., Exploring natural silk protein sericin for regenerative medicine: an injectable, photoluminescent, cell-adhesive 3D hydrogel, Sci. Rep. 4 (1) (2015) 7064, https://doi.org/10.1038/srep07064 (May).
[17] M.J. Jang, I.C. Um, Effect of sericin concentration and ethanol content on gelation behavior, rheological properties, and sponge characteristics of silk sericin, Eur. Polym. J. 93 (2017) 761–774, https://doi.org/10.1016/j.eurpolymj.2017.03.048.
[18] A. Veiga, I.V. Silva, M.M. Duarte, A.L. Oliveira, Current trends on protein driven bioinks for 3D printing, Pharmaceutics 13 (9) (2021) 1444, https://doi.org/10.3390/pharmaceutics13091444.
[19] Z. Wang, et al., Exploring natural silk protein sericin for regenerative medicine: an injectable, photoluminescent, cell-adhesive 3D hydrogel, Sci. Rep. 4 (1) (2015) 7064, https://doi.org/10.1038/srep07064 (May).
[20] C.S. Chen, et al., Three-dimensionally printed silk-sericin-based hydrogel scaffold: a promising visualized dressing material for real-time monitoring of wounds, ACS Appl. Mater. Interfaces 10 (40) (2018) 33879–33890, https://doi.org/10.1021/acsami.8b10072.
[21] S. Baptista-Silva, et al., In situ forming silk sericin-based hydrogel: a novel wound healing biomaterial, ACS Biomater. Sci. Eng. 7 (4) (2021) 1573–1586, https://doi.org/10.1021/acsbiomaterials.0c01745.
[22] Y. Zhang, et al., A sterile self-assembled sericin hydrogel via a simple two-step process, Polym. Test. 80 (2019), https://doi.org/10.1016/j.polymertesting.2019.106016.
[23] D.E. Chung, J.H. Lee, H. Kweon, K.-G. Lee, I.C. Um, Structure and properties of silk sericin obtained from different silkworm varieties, Int J. Indust Entomol. 30 (2) (2015) 81–85, https://doi.org/10.7852/ijie.2015.30.2.81.
[24] R.I. Kunz, R.M.C. Brancalhão, L.de F.C. Ribeiro, M.R.M. Natali, Silkworm sericin: properties and biomedical applications, Biomed. Res Int 2016 (2016) 1–19, https://doi.org/10.1155/2016/8175701 (vol).
[25] M.A. Serban, Translational biomaterials — the journey from the bench to the market — think 'product, Curr. Opin. Biotechnol. 40 (2016) 31–34, https://doi.org/10.1016/j.copbio.2016.02.009 (Aug).
[26] G.H. Altman, et al., Silk-based biomaterials, Biomaterials 24 (3) (2003) 401–416.
[27] F. Ahsan, T. Ansari, S. Usmani, P. Bagga, An insight on silk protein sericin: from processing to biomedical application, Drug Res 68 (06) (2018) 317–327, https://doi.org/10.1055/s-0043-121464.
[28] H. Teramoto, K. Nakajima, C. Takabayashi, Preparation of elastic silk sericin hydrogel, Biosci. Biotechnol. Biochem. 69 (4) (2005) 845–847, https://doi.org/10.1271/bbb.69.845.
[29] G. Tao, et al., Design and performance of sericin/poly(vinyl alcohol) hydrogel as a drug delivery carrier for potential wound dressing application, Mater. Sci. Eng. C. 101 (2019) 341–351, https://doi.org/10.1016/j.msec.2019.03.111.
[30] F.Y. Zhan, K.Y. Wang, M.M. Niu, Preparation and properties of glutaraldehyde cross-linked silk sericin films, Key Eng. Mater. 748 (2017) 148–152, https://doi.org/10.4028/www.scientific.net/KEM.748.148.
[31] C. Qi, et al., Photo-crosslinkable, injectable sericin hydrogel as 3D biomimetic extracellular matrix for minimally invasive repairing cartilage, Biomaterials 163 (2018) 89–104, https://doi.org/10.1016/j.biomaterials.2018.02.016.
[32] S. Baptista-Silva, et al., In situ forming silk sericin-based hydrogel: a novel wound healing biomaterial, ACS Biomater. Sci. Eng. 7 (4) (2021) 1573–1586, https://doi.org/10.1021/acsbiomaterials.0c01745.
[33] S. Baptista-Silva, et al., Exploring silk sericin for diabetic wounds: an in situ-forming hydrogel to protect against oxidative stress and improve tissue healing and regeneration, Biomolecules 12 (6) (2022) 801, https://doi.org/10.3390/biom12060801.
[34] X. Zhang, et al., Chemical modification of gelatin by a natural phenolic cross-linker, tannic acid, J. Agric. Food Chem. 58 (11) (2010) 6809–6815, https://doi.org/10.1021/jf1004226.
[35] S. Kong, R. Wang, S. Feng, D. Wang, Tannic acid as a natural crosslinker for catalyst-free silicone elastomers from hydrogen bonding to covalent bonding, Front Chem. 9 (2021), https://doi.org/10.3389/fchem.2021.778896.
[36] S.Y.Z. Moghaddam, E. Biazar, J. Esmaeili, B. Kheilnezhad, F. Goleij, S. Heidari, Tannic acid as a green cross-linker for biomaterial applications (Mini-Reviews), Med. Chem. 23 (13) (2023) 1320–1340, https://doi.org/10.2174/1389557522666220622112959.
[37] J.C. Warner, A.S. Cannon, K.M. Dye, Green chemistry, Environ. Impact Assess. Rev. 24 (7–8) (2004) 775–799, https://doi.org/10.1016/j.eiar.2004.06.006.
[38] A. Bigham, et al., Advances in tannic acid-incorporated biomaterials: Infection treatment, regenerative medicine, cancer therapy, and biosensing, Chem. Eng. J. 432 (2022) 134146, https://doi.org/10.1016/j.cej.2021.134146.
[39] E. Kim, J.-S. Jung, S.-G. Yoon, W.H. Park, Eco-friendly silk fibroin/tannic acid coacervates for humid and underwater wood adhesives, J. Colloid Interface Sci. 632 (2023) 151–160, https://doi.org/10.1016/j.jcis.2022.11.017.
[40] Y. Liu, et al., Healable and transparent ionic conductive hydrogels based on PNATF as multiple-signal sensors, ACS Appl. Polym. Mater. 7 (4) (2025) 2529–2540, https://doi.org/10.1021/acsapm.4c03794.
[41] J. Jing, S. Liang, Y. Yan, X. Tian, X. Li, Fabrication of hybrid hydrogels from silk fibroin and tannic acid with enhanced gelation and antibacterial activities, ACS Biomater. Sci. Eng. 5 (9) (2019) 4601–4611, https://doi.org/10.1021/acsbiomaterials.9b00604.
[42] R. Costa, et al., Modulation of VEGF signaling in a mouse model of diabetes by xanthohumol and 8-prenylnaringenin: unveiling the angiogenic paradox and metabolism interplay, Mol. Nutr. Food Res 61 (4) (2017) 1600488, https://doi.org/10.1002/mnfr.201600488.

[43] I. Guimarães, S. Baptista-Silva, M. Pintado, A. L. Oliveira, Polyphenols: a promising avenue in therapeutic solutions for wound care, Appl. Sci. 11 (3) (2021) 1230, https://doi.org/10.3390/app11031230.
[44] Y. Liu, et al., Fabrication of temperature and pH dual-sensitive semi-interpenetrating network hydrogel with enhanced adhesion and antibacterial properties, Polymer 326 (2025) 128343, https://doi.org/10.1016/j.polymer.2025.128343.
[45] Y.F. Cheng, et al., Tannic acid-assisted deposition of silk sericin on the titanium surfaces for antifouling application (Colloids and Interface Science Communications) 35 (2020) 100241, https://doi.org/10.1016/j.colcom.2020.100241. no. October 2019, p.
[46] Y. Zhang, J. Liu, L. Huang, Z. Wang, L. Wang, Design and performance of a sericin-alginate interpenetrating network hydrogel for cell and drug delivery, Sci. Rep. 5 (1) (2015) 12374, https://doi.org/10.1038/srep12374.
[47] J. Jing, S. Liang, Y. Yan, X. Tian, X. Li, Fabrication of hybrid hydrogels from silk fibroin and tannic acid with enhanced gelation and antibacterial activities, ACS Biomater. Sci. Eng. 5 (9) (2019) 4601–4611, https://doi.org/10.1021/acsbiomaterials.9b00604.
[48] J.U. Lee, M. Yeo, W.J. Kim, Y.W. Koo, G.H. Kim, Development of a tannic acid cross-linking process for obtaining 3D porous cell-laden collagen structure, Int J. Biol. Macromol. 110 (2018) 497–503, https://doi.org/10.1016/j.ijbiomac.2017.10.105.
[49] M.E. Carnes, C.R. Gonyea, R.G. Mooney, J.W. Njihia, J.M. Coburn, G.D. Pins, Horseradish peroxidase-catalyzed crosslinking of fibrin microthread scaffolds, Tissue Eng. Part C. Methods 26 (6) (2020) 317–331, https://doi.org/10.1089/ten.tec.2020.0083.
[50] A. Veiga, I.V. Silva, M.M. Duarte, A.L. Oliveira, Current trends on protein driven bioinks for 3D printing, Pharmaceutics 13 (9) (2021) 1444, https://doi.org/10.3390/pharmaceutics13091444.
[51] P.J.A.Ana L. Oliveira, Sara.B. Silva, Sandra C. Borges, 2018, Silk Sericin-based Hydrogel, Methods and Uses Thereof, WO/2018/011732.
[52] L.R. Almeida, et al., New biotextiles for tissue engineering: development, characterization and in vitro cellular viability, Acta Biomater. 9 (9) (2013) 8167–8181, https://doi.org/10.1016/j.actbio.2013.05.019.
[53] G. Asensio, M. Martín-del-Campo, R.A. Ramírez, L. Rojo, B. Vázquez-Lasa, New insights into the in vitro antioxidant routes and osteogenic properties of Sr/Zn phytate compounds, Pharmaceutics 15 (2) (2023) 339, https://doi.org/10.3390/pharmaceutics15020339.
[54] L.-L. Zuo, Z.-Y. Wang, Z.-L. Fan, S.-Q. Tian, J.-R. Liu, Evaluation of antioxidant and antiproliferative properties of three actinidia (Actinidia kolomikta, Actinidia arguta, Actinidia chinensis) extracts in vitro, Int J. Mol. Sci. 13 (5) (2012) 5506–5518, https://doi.org/10.3390/ijms13055506.
[55] V.P. Ribeiro, et al., Bioinspired silk fibroin-based composite grafts as bone tunnel fillers for anterior cruciate ligament reconstruction, Pharmaceutics 14 (4) (2022) 697, https://doi.org/10.3390/pharmaceutics14040697.
[56] K.M. Dupont, K. Sharma, H.Y. Stevens, J.D. Boerckel, A.J. García, R.E. Guldberg, Human stem cell delivery for treatment of large segmental bone defects, Proc. Natl. Acad. Sci. 107 (8) (2010) 3305–3310, https://doi.org/10.1073/pnas.0905444107.
[57] H. Yang, S. Yang, J. Kong, A. Dong, S. Yu, Obtaining information about protein secondary structures in aqueous solution using Fourier transform IR spectroscopy, Nat. Protoc. 10 (3) (2015) 382–396, https://doi.org/10.1038/nprot.2015.024.
[58] J. Kong, S. Yu, Fourier transform infrared spectroscopic analysis of protein secondary structures, Acta Biochim Biophys. Sin. 39 (8) (2007) 549–559, https://doi.org/10.1111/j.1745-7270.2007.00320.x.
[59] H. Susi, D.M. Byler, Resolution-enhanced fourier transform infrared spectroscopy of enzymes, Methods Enzymol. (1986) 290–311, https://doi.org/10.1016/0076-6879(86)30015-6.
[60] M. Jackson, H.H. Mantsch, The use and misuse of FTIR spectroscopy in the determination of protein structure, Crit. Rev. Biochem Mol. Biol. 30 (2) (1995) 95–120, https://doi.org/10.3109/10409239509085140.
[61] V.P. Ribeiro, et al., Bioinspired silk fibroin-based composite grafts as bone tunnel fillers for anterior cruciate ligament reconstruction, Pharmaceutics 14 (4) (2022) 697, https://doi.org/10.3390/pharmaceutics14040697.
[62] P.M. Gilbert, et al., Substrate elasticity regulates skeletal muscle stem cell self-renewal in culture, Science 329 (5995) (2010) 1078–1081, https://doi.org/10.1126/science.1191035 (Aug).
[63] M.P. Lutolf, P.M. Gilbert, H.M. Blau, Designing materials to direct stem-cell fate, Nature 462 (7272) (2009) 433–441, https://doi.org/10.1038/nature08602.
[64] C.A.P. Cass, K.J.L. Burg, Tannic acid cross-linked collagen scaffolds and their anti-cancer potential in a tissue engineered breast implant, J. Biomater. Sci. Polym. Ed. 23 (1–4) (2012) 281–298, https://doi.org/10.1163/092050610X550331.
[65] J.W. Bae, J.H. Choi, Y. Lee, K.D. Park, Horseradish peroxidase-catalysed in situ-forming hydrogels for tissue-engineering applications, J. Tissue Eng. Regen. Med 12 (3) (2014) 181–204, https://doi.org/10.1002/term.
[66] O. Olejnik, A. Masek, Natural phenolic compounds as modifiers for epoxidized natural rubber/silica hybrids, Molecules 27 (7) (2022) 2214, https://doi.org/10.3390/molecules27072214.
[67] F. Lee, K.H. Bae, M. Kurisawa, Injectable hydrogel systems crosslinked by horseradish peroxidase, Biomed. Mater. 11 (1) (2015) 14101, https://doi.org/10.1088/1748-6041/11/1/014101.
[68] R. JIN, C. HIEMSTRA, Z. ZHONG, J. FEIJEN, Enzyme-mediated fast in situ formation of hydrogels from dextran–tyramine conjugates, Biomaterials 28 (18) (2007) 2791–2800, https://doi.org/10.1016/j.biomaterials.2007.02.032.
[69] K.M. Park, K.S. Ko, Y.K. Joung, H. Shin, K.D. Park, In situ cross-linkable gelatin–poly(ethylene glycol)–tyramine hydrogel via enzyme-mediated reaction for tissue regenerative medicine, J. Mater. Chem. 21 (35) (2011) 13180, https://doi.org/10.1039/c1jm12527c.
[70] L.J. Zhu, M. Arai, K. Hirabayashi, Gelation of silk sericin and physical properties of the gel, J. Sericultural Sci. Jpn. 64 (5) (1995) 415–419, https://doi.org/10.11416/kontyushigen1930.64.415.
[71] J. Sparkes, C. Holland, The rheological properties of native sericin, Acta Biomater. 69 (2018) 234–242, https://doi.org/10.1016/j.actbio.2018.01.021.
[72] G. Stojkov, Z. Niyazov, F. Picchioni, R.K. Bose, Relationship between structure and rheology of hydrogels for various applications, Gels 7 (4) (2021), https://doi.org/10.3390/gels7040255.
[73] E. Quigley, J. Johnson, W. Liyanage, B.L. Nilsson, Impact of gelation method on thixotropic properties of phenylalanine- derived supramolecular hydrogels, Soft Matter (2020) 1–32, https://doi.org/10.1039/D0SM01217C.
[74] S. Gou, et al., Injectable, thixotropic, and multiresponsive silk fibroin hydrogel for localized and synergistic tumor therapy, ACS Biomater. Sci. Eng. 6 (2) (2020) 1052–1063, https://doi.org/10.1021/acsbiomaterials.9b01676.
[75] R. Barbucci, G. Leone, S. Lamponi, Thixotrophy property of hydrogels to evaluate the cell growing on the inside of the material bulk (Amber effect), J. Biomed. Mater. Res B Appl. Biomater. 76B (1) (2006) 33–40, https://doi.org/10.1002/jbm.b.30390.
[76] J. Aleman, Engineering a thixotropic and biochemically tunable hyaluronan and collagen bioink for biofabrication of multiple tissue construct types, 10.1101/2021.09.01.458584.
[77] R. Cui, et al., Polysaccharide-based hydrogels for wound dressing: design considerations and clinical applications, Front. Bioeng. Biotechnol. 10 (2022), https://doi.org/10.3389/fbioe.2022.845735.
[78] G. Dabiri, E. Damstetter, T. Phillips, Choosing a wound dressing based on common wound characteristics, Adv. Wound Care 5 (1) (2016) 32–41, https://doi.org/10.1089/wound.2014.0586.
[79] Z. Guo, et al., Tannic acid-based metal phenolic networks for bio-applications: a review, J. Mater. Chem. B 9 (20) (2021) 4098–4110, https://doi.org/10.1039/D1TB00383F.
[80] L.M. Yusiati, A. Kurniawati, C. Hanim, M.A. Anas, Protein binding capacity of different forages tannin, IOP Conf. Ser. Earth Environ. Sci. 119 (2018) 012007, https://doi.org/10.1088/1755-1315/119/1/012007.
[81] A. Scarano, et al., The chelating ability of plant polyphenols can affect iron homeostasis and gut microbiota, Antioxidants 12 (3) (2023) 630, https://doi.org/10.3390/antiox12030630.
[82] W. Chua, S.E. Poh, H. Li, Secretory proteases of the human skin microbiome, Infect. Immun. 90 (1) (2022), https://doi.org/10.1128/IAI.00397-21.
[83] G. Decante, R.L. Reis, J. Silva-Correia, J.M. Oliveira, Enzymatic crosslinked hydrogels, in: Hydrogels for Tissue Engineering and Regenerative Medicine, Elsevier, 2024, pp. 199–212, https://doi.org/10.1016/B978-0-12-823948-3.00046-4 (in).
[84] B. Poljsak, D. Šuput, I. Milisav, Achieving the balance between ROS and antioxidants: when to use the synthetic antioxidants, Oxid. Med Cell Longev. 2013 (2013) 1–11, https://doi.org/10.1155/2013/956792 (vol).
[85] X. Zhou, et al., Carboxymethyl chitosan/tannic acid hydrogel with antibacterial, hemostasis, and antioxidant properties promoting skin wound repair, ACS Biomater. Sci. Eng. 9 (1) (2023) 437–448, https://doi.org/10.1021/acsbiomaterials.2c00997.
[86] Y. Zhang, et al., A sterile self-assembled sericin hydrogel via a simple two-step process, Polym. Test. 80 (2019), https://doi.org/10.1016/j.polymertesting.2019.106016.
[87] N. Sahiner, S. Sagbas, M. Sahiner, C. Silan, N. Aktas, M. Turk, Biocompatible and biodegradable poly(Tannic Acid) hydrogel with antimicrobial and antioxidant properties, Int J. Biol. Macromol. 82 (2016) 150–159, https://doi.org/10.1016/j.ijbiomac.2015.10.057.
[88] A. Veiga, F. Castro, F. Rocha, A. Oliveira, Protein-based Hydroxyapatite materials: tuning composition towards biomedical applications, ACS Appl. Bio Mater. (2020), https://doi.org/10.1021/acsabm.0c00140 p. acsabm.0c00140, Apr.
[89] A. Veiga, F. Castro, F. Rocha, A.L. Oliveira, Recent advances in silk sericin/calcium phosphate biomaterials, Front. Mater. 7 (2020) 1–14, https://doi.org/10.3389/fmats.2020.00024 (no. February).
[90] P. Mhlanga, P.O. Perumal, A.M. Somboro, D.G. Amoako, H.M. Khumalo, R. B. Khan, Mechanistic insights into oxidative stress and apoptosis mediated by tannic acid in human liver hepatocellular carcinoma cells, Int J. Mol. Sci. 20 (24) (2019) 6145, https://doi.org/10.3390/ijms20246145.
[91] N. SP, et al., Tannic acid inhibits non-small cell lung cancer (NSCLC) stemness by inducing G 0 /G 1 cell cycle arrest and intrinsic apoptosis, Anticancer Res 40 (6) (2020) 3209–3220, https://doi.org/10.21873/anticanres.14302.
[92] M. Bercea, Rheology as a tool for fine-tuning the properties of printable bioinspired gels, Molecules 28 (6) (2023) 2766, https://doi.org/10.3390/molecules28062766.
[93] J. Espinosa-Rivero, C. Bañuelos, A. Betanzos, Impact of cell–cell interactions on communication and collectiveness, in: Cell Movement in Health and Disease, Elsevier, 2022, pp. 51–65, https://doi.org/10.1016/B978-0-323-90195-6.00005-X (in).
[94] J.B. Costa, J. Silva-Correia, J.M. Oliveira, R.L. Reis, Fast setting silk fibroin bioink for bioprinting of patient-specific memory-shape implants, Adv. Health Mater. 6 (22) (2017) 1701021, https://doi.org/10.1002/adhm.201701021.
[95] L.-P. Yan, et al., Tumor growth suppression induced by biomimetic silk fibroin hydrogels, Sci. Rep. 6 (1) (2016) 31037, https://doi.org/10.1038/srep31037.
[96] O. Hasturk, K.E. Jordan, J. Choi, D.L. Kaplan, Enzymatically crosslinked silk and silk-gelatin hydrogels with tunable gelation kinetics, mechanical properties and

bioactivity for cell culture and encapsulation, Biomaterials 232 (2020) 119720, https://doi.org/10.1016/j.biomaterials.2019.119720.
[97] W. Pudkon, C. Laomeephol, S. Damrongsakkul, S. Kanokpanont, J. Ratanavaraporn, Comparative study of silk fibroin-based hydrogels and their potential as material for 3-dimensional (3D) printing, Molecules 26 (13) (2021) 3887, https://doi.org/10.3390/molecules26133887.
[98] R. Andreazza, A. Morales, S. Pieniz, J. Labidi, Gelatin-based hydrogels: potential biomaterials for remediation, Polymer 15 (4) (2023) 1026, https://doi.org/10.3390/polym15041026.
[99] E. Devernois, T. Coradin, Synthesis, characterization and biological properties of type i collagen–chitosan mixed hydrogels: a review, Gels 9 (7) (2023) 518, https://doi.org/10.3390/gels9070518.
[100] R. Meng, et al., Research progress on albumin-based hydrogels: properties, preparation methods, types and its application for antitumor-drug delivery and tissue engineering, Front. Bioeng. Biotechnol. 11 (2023), https://doi.org/10.3389/fbioe.2023.1137145.
[101] N. Singh, M. Kumar, J.F. Miravet, R.V. Ulijn, B. Escuder, Peptide-based molecular hydrogels as supramolecular protein mimics, Chem. A Eur. J. 23 (5) (2017) 981–993, https://doi.org/10.1002/chem.201602624.
[102] M. Ghosh, M. Halperin-Sternfeld, I. Grinberg, L. Adler-Abramovich, Injectable alginate-peptide composite hydrogel as a scaffold for bone tissue regeneration, Nanomaterials 9 (4) (2019) 497, https://doi.org/10.3390/nano9040497.
[103] G. Ochbaum, M. Davidovich-Pinhas, R. Bitton, Tuning the mechanical properties of alginate–peptide hydrogels, Soft Matter 14 (21) (2018) 4364–4373, https://doi.org/10.1039/C8SM00059J.
[104] S. Koutsopoulos, S. Zhang, Long-term three-dimensional neural tissue cultures in functionalized self-assembling peptide hydrogels, matrigel and collagen I, Acta Biomater. 9 (2) (2013) 5162–5169, https://doi.org/10.1016/j.actbio.2012.09.010.
[105] X.-M. Zhou, et al., Enzymatically active microgels from self-assembling protein nanofibrils for microflow chemistry, ACS Nano 9 (6) (2015) 5772–5781, https://doi.org/10.1021/acsnano.5b00061.
[106] G. Eke, N. Mangir, N. Hasirci, S. MacNeil, V. Hasirci, Development of a UV crosslinked biodegradable hydrogel containing adipose derived stem cells to promote vascularization for skin wounds and tissue engineering, Biomaterials 129 (2017) 188–198, https://doi.org/10.1016/j.biomaterials.2017.03.021.
[107] N.-C. Cheng, W.-J. Lin, T.-Y. Ling, T.-H. Young, Sustained release of adipose-derived stem cells by thermosensitive chitosan/gelatin hydrogel for therapeutic angiogenesis, Acta Biomater. 51 (2017) 258–267, https://doi.org/10.1016/j.actbio.2017.01.060.
[108] S. Chen, et al., Mesenchymal stem cell-laden anti-inflammatory hydrogel enhances diabetic wound healing, Sci. Rep. 5 (1) (2015) 18104, https://doi.org/10.1038/srep18104.
[109] Y. Wang, et al., A biomimetic silk fibroin/sodium alginate composite scaffold for soft tissue engineering, Sci. Rep. 6 (1) (2016) 39477, https://doi.org/10.1038/srep39477.
[110] F. Fan, S. Saha, D. Hanjaya-Putra, Biomimetic hydrogels to promote wound healing, Front Bioeng. Biotechnol. 9 (2021) 1–24, https://doi.org/10.3389/fbioe.2021.718377 (no. September).
[111] E. Mancha Sánchez, et al., Hydrogels for bioprinting: a systematic review of hydrogels synthesis, bioprinting parameters, and bioprinted structures behavior, Front. Bioeng. Biotechnol. 8 (2020), https://doi.org/10.3389/fbioe.2020.00776 (no. August).
[112] S. Prete, M. Dattilo, F. Patitucci, G. Pezzi, O.I. Parisi, F. Puoci, Natural and synthetic polymeric biomaterials for application in wound management, J. Funct. Biomater. 14 (9) (2023) 455, https://doi.org/10.3390/jfb14090455.
[113] V.K. Vendra, L. Wu, S. Krishnan, Polymer Thin Films for Biomedical Applications, in: Nanotechnologies for the Life Sciences, Wiley, 2010, https://doi.org/10.1002/9783527610419.ntls0179 (in).
[114] Quarta Zafar, Ragusa Marradi, Recent developments in the reduction of oxidative stress through antioxidant polymeric formulations, Pharmaceutics 11 (10) (2019) 505, https://doi.org/10.3390/pharmaceutics11100505.
[115] N.I.M. Fadilah, et al., Antioxidant biomaterials in cutaneous wound healing and tissue regeneration: a critical review, Antioxidants 12 (4) (2023) 787, https://doi.org/10.3390/antiox12040787.
[116] S.M. McCarty, S.L. Percival, Proteases and delayed wound healing, Adv. Wound Care 2 (8) (2013) 438–447, https://doi.org/10.1089/wound.2012.0370.
[117] W. He, et al., Sealing the pandora's vase of pancreatic fistula through entrapping the digestive enzymes within a dextrorotary (D)-peptide hydrogel, Nat. Commun. 15 (1) (2024) 7235, https://doi.org/10.1038/s41467-024-51734-7.
[118] T. Ting, C. Yu, Yu Zhang, The potential of silk sericin protein as a serum substitute or an additive in cell culture and cryopreservation, Amino Acids 49 (6) (2017) 1029–1039, https://doi.org/10.1007/s00726-017-2396-3.
[119] P. Marrazzo, C. O'leary, Repositioning natural antioxidants for therapeutic applications in tissue engineering, Bioengineering 7 (3) (2020) 1–35, https://doi.org/10.3390/bioengineering7030104.
[120] A. Loewa, J.J. Feng, S. Hedtrich, Human disease models in drug development, Nat. Rev. Bioeng. 1 (8) (2023) 545–559, https://doi.org/10.1038/s44222-023-00063-3.
[121] X. Li, et al., Three-dimensional sulfated bacterial cellulose/gelatin composite scaffolds for culturing hepatocytes, Cyborg Bionic Syst. 4 (2023), https://doi.org/10.34133/cbsystems.0021.
[122] C. Dannert, B.T. Stokke, R.S. Dias, Nanoparticle-hydrogel composites: from molecular interactions to macroscopic behavior, Polymer 11 (2) (2019) 275, https://doi.org/10.3390/polym11020275.